International Journal of Concrete Structures and Materials

RESEARCH

Open Access

High-Strength Self-Compacting Concrete Production Incorporating Supplementary Cementitious Materials: Experimental Evaluations and Machine Learning Modelling

Md. Habibur Rahman Sobuz[1,2*], Fahim Shahriyar Aditto[1], Shuvo Dip Datta[3], Md. Kawsarul Islam Kabbo[3], Jannat Ara Jabin[1], Md. Munir Hayet Khan[2], S. M. Arifur Rahman[4], Mehernaz Raazi[1] and Ahmad Akib Uz Zaman[5]

Abstract

This study investigates mechanical properties, durability performance, non-destructive testing (NDT) characteristics, environmental impact evaluation, and advanced machine learning (ML) modelling techniques employed in the analysis of high-strength self-compacting concrete (HSSCC) incorporating varying supplementary cementitious materials (SCMs) to develop sustainable building construction. The findings from the fresh characteristics test indicate that mixes' optimal flowability and passing qualities can be achieved using different concentrations of marble powder (MP) alongside a consistent amount of silica fume (SF) and fly ash (FA). Moreover, the incorporation of 10% MP along with 10% FA and 20% SF in HSSCC significantly improved the compressive strength by 14.68%, while the splitting tensile strength increased by 15.59% compared to the reference mix at 56 days. While random forest (RF), gradient boosting (GB), and their ensemble models exhibit strong coefficient correlation (R^2) values, the GB model demonstrates more precision, indicating reliable predicted outcomes of the mechanical properties. Following subsequent testing, it has been demonstrated that incorporating SCMs improves the NDT properties of HSSCC and enhances its durability. The finer MP, SF, and FA particles enhanced microstructural performance by minimizing voids and cracks while improving the C–H–S bond. As noticed by its lower CO_2-eq per MPa for SCMs, the HSSCC mix with up to 15% MP inclusion increased mechanical strength while reducing the environmental footprint, making it an eco-friendly concrete alternative.

Keywords Sustainable high-strength self-compacting concrete, Marble powder, Mechanical properties, Machine learning modelling, Durability properties, Non-destructive characteristics

Journal information: ISSN 1976-0485 / eISSN 2234-1315.

*Correspondence:
Md. Habibur Rahman Sobuz
habib@becm.kuet.ac.bd
Full list of author information is available at the end of the article

1 Introduction

Concrete is one of the most frequently utilized materials for construction purposes in every nation because of its exceptional structural stability and durability. A highly dispersed aggregate, cement, and water mixture makes concrete. The aggregate may impact efficiency and durability of concrete, but the strength of concrete may also be constrained. Reusing waste materials is an effort the engineering community makes to preserve natural resources (Yong and Lee, 2022; Raghunath et al., 2019). In-depth research on the root cause as well as the consequences of concrete degradation is necessary before placing concrete in various sites. There is a substantial durability issue in places like marine environments, underground, etc., due to assault from carbonation, sulphate, acid, and chloride. Self-compacting concrete (SCC) is a clear solution to the aforementioned issue.

There have been numerous studies investigating various partial cement alternatives for SCC (Khan et al., 2023; Rahman Sobuz et al., 2023; Sadek et al., 2016; Hasan et al., 2022). If the investigation illustrates that using marble powder (MP) as an inorganic addition adhering to SCC is acceptable and effective, that may also be a preferred disposal approach. The potential applications of MP, including enhancing soil, the approach to hydrogenation, asphalt placement, pottery, ceramics, thermoset epoxy composites, and polymeric manufacturing methods, have all been investigated in recent years (Aruntaș et al., 2010). Numerous studies recommend the incorporation of MP as a substitute for cement in cementitious materials (Aditto et al., 2023; Aliabdo et al., 2014; Elyamany et al., 2014). Meera et al. (2020) investigated the use of marble powder in SCC revealing positive results. According to the study performed on SCC, Lija and Minu (2016) concluded that replacing cement with a mixture of 15% marble waste and 15–30% silica fume strengthened the flexural strength and stiffness. Additionally, the durability and the chloride resistance of ternary combined SCC comprising large-scale fly ash and silica fume were experimentally investigated by Wongkeo et al. (2014) and they reported that the integration of fly ash in SCC considerably increased the durability qualities. Utilizing fly ash ranging from 10 to 50%, Dhiyaneshwaran et al. (2013) conducted a study presenting improved durability. El-Chabib and Syed (2013) also investigated the impact of a quaternary mix, including additional cementitious elements. The findings suggested that concrete having 10% silica fume (SF) provided enhanced compressive strength. The durability characteristics associated with normal strength self-compacting concrete and their impact on RC construction were examined experimentally by Sideris and Anagnostopoulos (2013). The outcomes were contrasted with concrete that had been vibrated traditionally. Researchers Vasusmitha and Rao (2013) looked at how various mineral additives affected the compression and permeation of HSSCC. According to the findings, HSSCC had less chloride permeability onto concrete, a greater bond and strength against tension, less oxygen permeability, and less plastic settling.

Moreover, sorptivity, porosity, and chloride ion permeability tests were used by Kanellopoulos et al. (2012) to examine the durability characteristics of SCC and traditional concrete. Tennich et al. (2017) evaluated SCC's durability, utilizing tile and marble wastes that sulphates had attacked. Leung et al. (2016) reported using SF and FA in combination for SCC. Higher resistance was observed when the researchers evaluated the implications of SF and FA on the sorptivity characteristics of SCC. Using proportions of 0–30% of the entire amount of cement volume, Sardinha et al. (2016) replaced the MP. They claimed that MP replacement in cement produced an approximate compressive strength. Likewise, Ahmad et al. (2023) replaced cement with marble waste which resulted in a 20% increase in compressive strength and durability. The MP and the marble tile fragments were added to the SCC by Tennich et al. (2015) as filler. According to their findings, adding MP enhanced the compressive and tensile strength of the material. Jalal et al. (2015) examined the impact of fly ash, silica fume, and nano-silica on the hardened characteristics of a superior-performance SCC. The influence of marble powder (MP) on the strength of compression of SCC was examined by Uysal and Tanyildizi (2012). According to Jain et al. (2013), combining data from ultrasonic pulse velocity testing and Schmidt hammer tests provided a more precise way to calculate the compressive strength of concrete than depending just on the outcomes of distinct experiments. Belouadah et al. (2021) further explored the potential for non-destructive methods to evaluate the physico-mechanical characteristics of concrete using MP and obtained positive results for up to 10% MP replacement. Furthermore, using a non-destructive test and marble sand powder ranging from 5 to 25%, Velci Shridevi et al. (2023) assessed the strength qualities of SCC and discovered increased strength after 28 days. According to Breysse (2012), it is possible to determine the compressive strength of concrete using either the Schmidt hammer or ultrasonic pulse velocity assessments individually or together.

In the construction industry, artificial intelligence and machine learning are advanced techniques to quantify the fresh and mechanical properties of SCC using formulated mixture ratios, focusing on various strength predictions (Ahmad et al., 2021; Datta et al., 2024; Habibur Rahman Sobuz et al., 2024; Xie et al., 2020). ML approaches can accurately predict

mechanical characteristics, enabling tasks like classification, correlation, regression, clustering, and enhancing the mechanical as well as fresh properties of concrete (Silva et al., 2020; Xu et al., 2019). Azimi-Pour et al. (2020) employed a support vector machine to evaluate the fresh and mechanical properties of SCC, incorporating fly ash as a potential substitute for cement. Asadi Shamsabadi et al. (2022) reported that ML models using XGBoost and ANN informational models accurately predicted the compressive strength of WMP concrete with a high degree of reliability ($R^2 > 0.97$). The utilization of multiple machine learning models to forecast the compressive strength of SCC with the inclusion of marble powder and rice husk ash was reported by Mahmood et al. (2023). Efficient SCC mixture compositions and compressive strengths were part of the extensive dataset used to train the ANN model by Acikgenc Ulas (2023).

There have been relatively very few comprehensive studies addressing the combined impact of SF, FA, and MP SCMs in the production of HSSCC. However, the literature lacks comprehensive information regarding the combined effects of SCMs, such as FA, MP, and SF, on durability, non-destructive testing (NDTs), and machine learning (ML) modelling. Therefore, this study introduces several novel contributions to the field of HSSCC by exploring the synergistic effects of incorporating 0–20% MP alongside 20% SF and 10% FA as SCMs. This investigation provides a comprehensive analysis that not only evaluates the mechanical properties and durability of HSSCC but also explores ML modelling to predict these properties accurately compared to existing studies. The unique approach combines experimental evaluations with ML techniques viz. random forest (RF) and gradient boosting (GB) models, offering a novel perspective on the prediction of concrete properties, which has not been extensively covered in previous works. Moreover, the study brings to light the environmental benefits of utilizing SCMs by demonstrating a significant reduction in CO_2 emissions without compromising the mechanical efficiency of the concrete. A combined investigation into the microstructural characteristics and the interaction between destructive and non-destructive testing results, this study finds the opportunity to extend valuable insights into the optimization of HSSCC mixtures for sustainable construction practices. The rigorously designed experimental program including microstructural properties and a predictive ML model represents a pivotal step towards the use of SCMs in concrete research, particularly in achieving a balance between enhanced mechanical properties, durability, and environmental sustainability.

2 Materials

Locally produced Ordinary Portland Cement (OPC) of type-I, which followed BDS EN 197–1 (BDS.EN:197–1), was utilized for this study. The coarse aggregate originated as angular stone from a nearby source. The coarse aggregate used had an optimum size of 19 mm. Natural river sand passed through a 4.75 mm sieve and was employed as a fine aggregate (Astm, 2018). Silica fume was purchased from a local supplier in Dhaka, Bangladesh. Fly ash was obtained for free from a reputable cement manufacturer in Bangladesh. Marble powder was also collected free of cost from an industrial firm which is situated in Narayanganj, Bangladesh. A superplasticizer based on polycarboxylic ether was employed to achieve the requisite workability. Fig. 1 illustrates the gradation curve for marble powder (MP) as well as coarse and fine aggregate with lower and upper limits following ASTM C33 (ASTM-C33., 2003). The physical characteristics of materials provide several benefits, including strength, workability, durability, and chemical resistance. The physical features of the substances are presented in Table 1. The chemical reactions between the components influence the overall effectiveness of HSSCC, whereas fly ash lowers permeability, silica fume strengthens density, OPC hydrates, and marble powder improves strength. Table 2 illustrates the findings of an X-ray fluorescence (XRF) analysis that evaluated the chemical properties of OPC, MP, SF, and FA.

3 Experimental Program

3.1 Mix Design and Concrete Mixing

To investigate the characteristics of SCC in line with the standards established by the EFNARC, several concrete mixtures were created at a constant water-to-binder ratio of 0.36 with OPC, MP, FA, and SF at varied proportioning ratios (EFNARC, 2005). The mix proportions for every SCC batch are displayed in Table 3, whereas 'S' implies silica fume, 'F' implies fly ash, and 'M' implies marble powder content. To partially replace cement, MP, FA, and SF were utilized. The replacement rates of 0, 5, 10, 15, and 20% of MP in place of OPC enable an assessment of the impacts on concrete strength, durability, and other characteristics. Experimental conditions are kept consistent and uniform by maintaining consistent proportions of 10% FA and 20% SF, thereby isolating the implications of MP substitution. Also, in real-world scenarios, the availability and applicability of alternative materials for concrete production might change, which is reflected in the variation of MP proportions depending on waste materials. Through the consideration of these variables, the experimental design provides a thorough investigation of the influence of MP substitution on concrete qualities

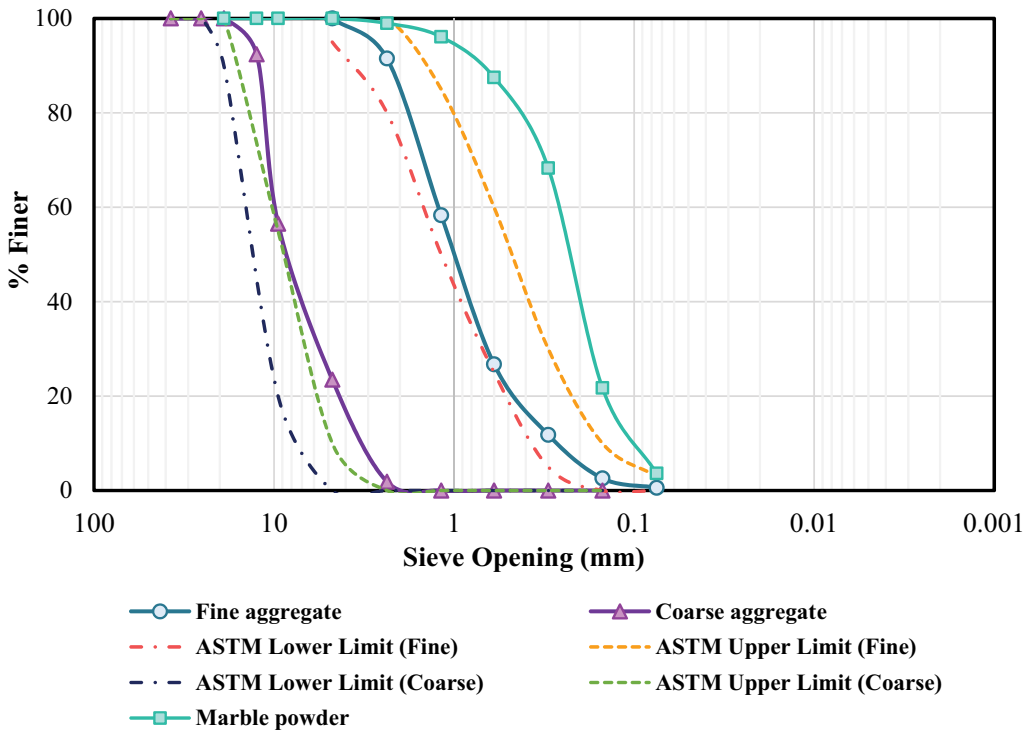

Fig.1 Gradation curve of marble powder, fine and coarse aggregate

Table 1 Characteristics of the substances of physical composition

Materials	Loose Unit Weight (Kg/m^3)	Fineness Modulus	Moisture Content (%)	Absorption (%)	Specific Gravity
Fine aggregate	1686.9	3.09	2.31	1.63	2.72
Coarse aggregate	1640.69	5.26	1.79	1.17	2.93
OPC	1440	–	–	–	3.15
Marble powder	1375	–	–	–	2.71
Fly ash	1115	–	–	–	2.10
Silica fume	600	–	–	–	2.22

Table 2 Chemical compositions of cement (OPC), fly ash (FA), marble powder (MP), and silica fume (SF)

Properties	OPC (%)	FA (%)	SF (%)	MP (%)
SiO_2	19.01	61.53	89.94	5.98
Al_2O_3	4.51	30.47	0.64	0.46
Fe_2O_3	3.2	1.24	0.79	0.21
CaO	66.89	1.31	0.75	46.31
MgO	1.23	0.89	1.52	7.06
SO_3	0.45	0.31	0.09	0.17
K_2O	2.53	0.42	0.58	1.78
Na_2O	1.10	0.49	0.43	2.19
LOI	1.13	3.37	5.26	35.85

while preserving uniformity and practical applicability. The control mix called S20F0M0 contains 20% SF, 0% FA, and 0% MP.

3.2 Preparing and Curing Samples

The compressive, splitting tensile strength, and water permeability evaluations were performed on cylindrical molds measuring 100 × 200 mm. Concrete discs 100 mm in diameter and 50 mm thick were saw-cut from 100 × 200 mm cylinders as the samples for the sorptivity and RCPT tests. After 24 h in an area having an average temperature of about 27 ± 4 °C, samples were taken out and labelled for easier identification. The samples were submerged completely using potable water and cured

Table 3 Mix proportion for all SCC mixtures

Mix ID	Mix nature	Water (kg/m^3)	OPC (kg/m^3)	Marble powder (kg/m^3)	Fly ash (kg/m^3)	Silica fume (kg/m^3)	Fine aggregate (kg/m^3)	Coarse aggregate (kg/m^3)	SP (%)
S20F0M0	Binary	198	440	–	–	110	962.5	797.5	1.2
S20F10M0	Ternary	198	385	–	55	110	962.5	797.5	1.2
S20F10M5	Quaternary	198	357.5	27.5	55	110	962.5	797.5	1.2
S20F10M10	Quaternary	198	330	55	55	110	962.5	797.5	1.2
S20F10M15	Quaternary	198	302.5	82.5	55	110	962.5	797.5	1.2
S20F10M20	Quaternary	198	275	110	55	110	962.5	797.5	1.2

for 7, 28, and 56 days using a plastic treatment chamber. Each specimen was assembled and cured in a laboratory per ASTM-C192/C192M-18 (ASTM-C192/192 M).

3.3 Evaluation Practice

According to the BS EN 12350–8 (BS.EN:12350–8, 2010) and BS EN 12350–12 (EN.BS:12350–12, 2010) regulations, flowability and passing ability of fresh materials were assessed using the slump flow and J-ring flow tests. Experimental methods for verifying all fresh qualities are shown in Fig. 2a, b.

The compressive strength test was performed in line with ASTM C39 standards (ASTM-C39, 2010) to evaluate the cylinder specimen in this investigation. To examine the influence of FA, MP, and SF regarding the compressive strength of HSSCC, cylindrical molds with dimensions of 100 × 200 mm were selected after undergoing water curing for durations of 7, 28, and 56 days. The cylinder specimen used in this investigation was tested using the splitting tensile test in compliance with the ASTM C496 standard (ASTM-C496, 2011). This would be conducted as the same procedure as the compressive strength test.

Fig. 2e depicts the procedure used to evaluate water permeability following BS EN 12390–8 (EN.BS-12390–8, 2019). HSSCC specimens were subjected to sorptivity testing following ASTM-C 1585–13 (ASTM-C1585, 2013), as highlighted in Fig. 2f. According to the ASTM C1202 (ASTM-C, 1202, 2019) Rapid Chloride Penetration Test (RCPT), a concrete specimen saturated with water is exposed to a 60 V DC voltage for 6 h, incorporating the apparatus and cells indicated in Fig. 2g.

The compressive strength for each NDT sample was assessed using the digital rebound hammer test following ASTM C805 (ASTM-C805, 2018), which is illustrated in Fig. 2h at 28, and 56 days after curing the process. Ultrasonic pulse velocity (UPV) experiments were carried out to analyze the pulse velocities at 28 and 56 days following ASTM C597 (ASTM-C597, 2009), as can be seen in Fig. 2i. In Table 4, the RCPT, the rebound number, and the UPV were utilized to define the charge passed as well as concrete quality in structures.

Microstructural properties were assessed using a scanning electron microscope (SEM) in compliance with ASTM C1723-16 (ASTM-C, 1723, 2016). The hardened concrete specimens were analyzed under a scanning electron microscope to understand the compactness of the interfacial transition zone. The concrete specimens were cut into 5 × 5 mm sizes and soaked in isopropanol for 72 h, followed by drying at 40 °C. Later, the concrete specimens were vacuum desiccated for 24 h coated with 5 nm carbon and analyzed at 15 keV voltage and beam intensity of 14.0 under an SE detector at high vacuum (S. A. Rahman et al., 2023a, 2023b, 2024).

3.4 Predictive Machine Learning Ensemble Model

Researchers have developed ensemble methods to enhance prediction accuracy, which merges several machine learning (ML) models into a single predictive model (Al Daoud, 2019). Ensemble methods, like boosting and bagging, which combine RF and GB algorithms, provide satisfactory outcomes. Equations 1, 2, 3, 4 were implemented to evaluate the impact of the model utilizing multiple metrics. Fig. 3 depicts the framework executed in this investigation to generate both single-based machine learning and ensemble model algorithms.

$$R^2 = 1 - \frac{\sum_{i=1}^{n} (Y - Y_i)^2}{\sum_{i=1}^{n} Y_i^2} \tag{1}$$

$$MAE = \frac{1}{n} \sum_{i=1}^{n} |Y - Y_i|^2 \tag{2}$$

$$RMSE = \sqrt{\frac{1}{n} \sum_{i=1}^{n} (Y - Y_i)^2} \tag{3}$$

Fig. 2 Test setup on HSSCC of (**a**) slump flow (**b**) J-ring flow (**c**) compressive strength (**d**) splitting tensile strength (**e**) water permeability (**f**) sorptivity (**g**) RCPT (**h**) rebound hammer and (**i**) UPV assessment

Table 4 RCPT, rebound number and velocity criterion for concrete

Charge passed (coulombs)	Chloride ion penetrability	Rebound number	Quality of concrete	Pulse velocity (km/sec)	Concrete quality grading
> 4000	High	> 40	Very Good Hard Layer	> 4.5	Excellent
2000–4000	Moderate	30–40	Good Layer	3.5–4.5	Good
1000–2000	Low	20–30	Fair	3–3.5	Medium
100–1000	Very low	< 20	Poor Concrete	< 3	Doubtful
< 100	Negligible	0	Delaminated	–	–

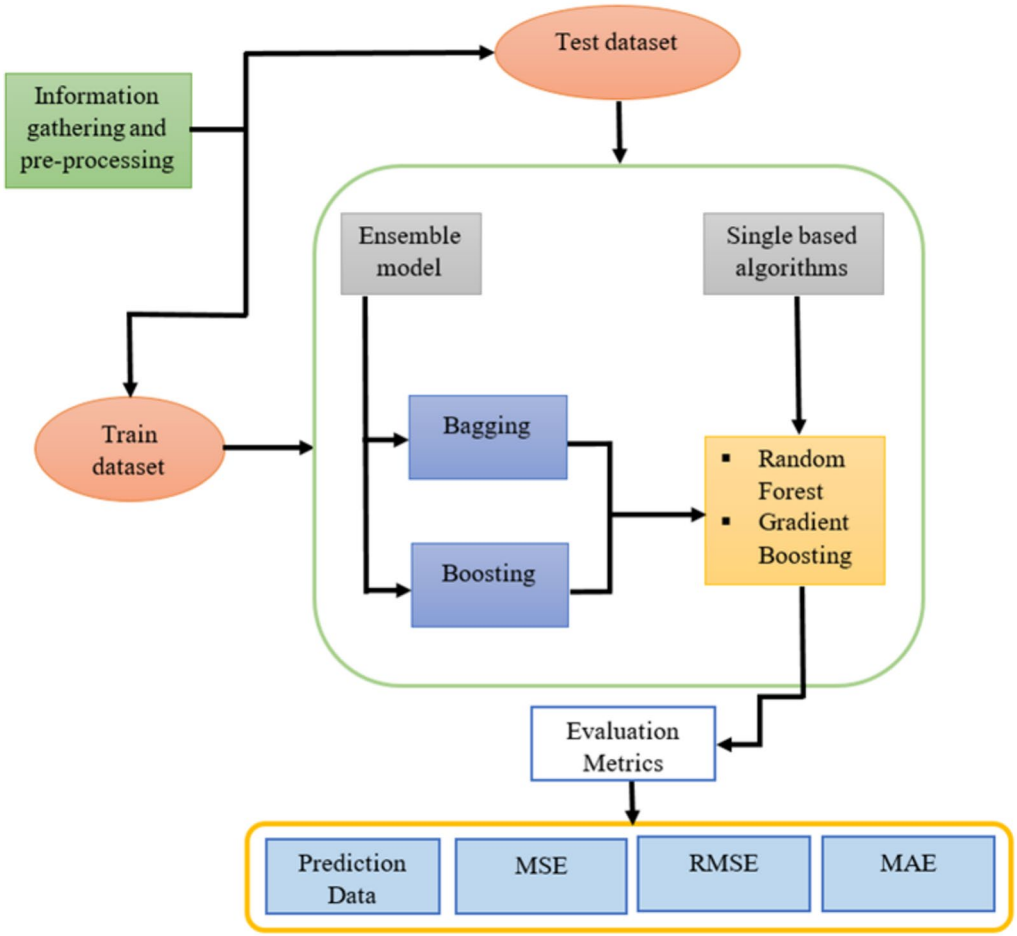

Fig. 3 Flowchart diagram for the proposed ML approach

$$\mathrm{MSE} = \frac{1}{n}\sum_{i=1}^{n}(Y - Y_i)^2 \tag{4}$$

where R^2 = correlation coefficient, MAE = mean absolute error, RMSE = root mean square error, and MSE = mean square error.

The random forest (RF), established by Leo Breiman in 2001 by integrating classification and regression trees with bagging, is one type of decision tree that delivers the most enhanced presentation when predicting the outcome (Breiman, 2001). When used as a predictive estimator, RF considers extensive randomized decision trees and updates them through data from various subsets of the training data. By smoothing out the variations and biases of individual trees, this approach lessens overfitting and enhances generalization.

Gradient boosting (GB) progressively creates an ensemble by repeatedly training a new model to emphasize improperly organized training data from previous approaches. Jerome H. Friedman discovered gradient boosting, a method for developing strong prediction models that can efficiently deal with complicated patterns and linkages in the information (Friedman, 2002). GB is nowadays a widely applied algorithm because of its capacity to attain accuracy levels and manage multiple data categories.

With a dataset of mixed compositions and experimental values, the accompanying Python script uses scikit-learn to train and assess two ML models: RF and GB. The models are trained and utilized for prediction-making after the data has been loaded and prepared. The forecasts from both models are then averaged to provide an ensemble prediction. This procedure is carried out in a Python environment using libraries like scikit-learn for machine learning methods, pandas for data processing, and numpy for mathematical operations. The syntax is procedural, meaning that the script is organized sequentially, beginning with the import of required libraries and ending with the presentation of the results. Splitting the

dataset into training, testing, and validation subsets is an important step in this procedure. The function mentioned in the supplied script divides the dataset at random into training and testing sets in a predetermined proportion. Through the use of data splitting methods such as train_test_split, the Python code may improve the overall resilience and dependability of the ML process and guarantee a more accurate model assessment.

4 Results and Discussion

4.1 Effects of the Fresh Characteristics of HSSCC

4.1.1 Slump Flow and J-Ring Test

Fig. 4 illustrates the J-ring and slump flowing for the reference mix and several additional SCC combinations. The slump rates appeared within 675–740 mm, per the accepted criteria governing HSSCC slump flow established by the European Federation of National Associations Representing for Concrete (EFNARC) (EFNARC, 2005). Slump flow analysis showed that mixture S20F10M10 had an optimal value of 740 mm instead of the control mixture's 675 mm. Additional analysis noticed the slump's flow rates for each of the mixes, including 0, 5, 10, 15, and 20% MP, in addition to the steady 10% FA and 20% SF, were 1.85, 7.40, 9.60, 5.90, and 5% higher than the control mixture S20F0M0, respectively. The increase in performance may be associated with the finer particles of MP, which generate less friction internally and occur in a smoother flow. The maximum slump rate was recorded at 20% substitution, as Choudhary et al. (2019) found that the flow rate of slump enhanced with each additional MP substitution as well as exceeding 655 mm.

In contrast, the J-ring flow value enhancement was detected when marble powder was included in the HSSCC combinations. It was found that the optimal J-ring flow measurement for the S20F10M10 combination appeared to be 715 mm, which came very close to the slump value of 740 mm. When compared to the control mix, the J-ring flow measurements increased by 4.18, 11.68, 19.17, 16.59, and 15% in a combination that included 0, 5, 10, 15, and 20% replacement of MP alongside 10 and 20% FA and SF, accordingly. Particles of the small size of MP, FA, and SF fill out the pores along with voids among coarse particles forming a more homogeneous mixture that can flow easily inside the J-ring with no separating. An almost identical investigation was performed by Belaidi et al. (2016), who found that adding natural pozzolana and marble powder as alternatives to OPC improved the passing ability of SCC mixtures.

4.1.2 Predictive Analysis of ML Algorithms on Fresh Properties

The effectiveness of the generated models was evaluated by their ability to quantify the slump flow and HSSCC J-ring assessment. In addition, a well-trained model can generate accurate predictions of slump flow and J-ring values for the input data. The intricate relationships between input parameters and the corresponding slump flow and J-ring values were effectively captured in the models by employing ML methodologies. This approach

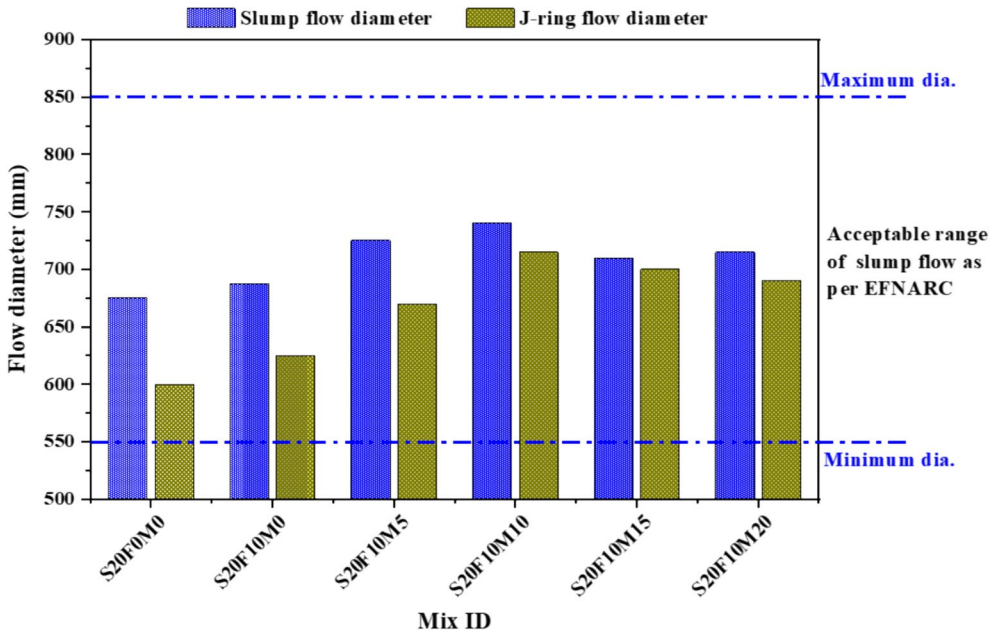

Fig. 4 Slump flow and J-ring flow rates of HSSCC specimens

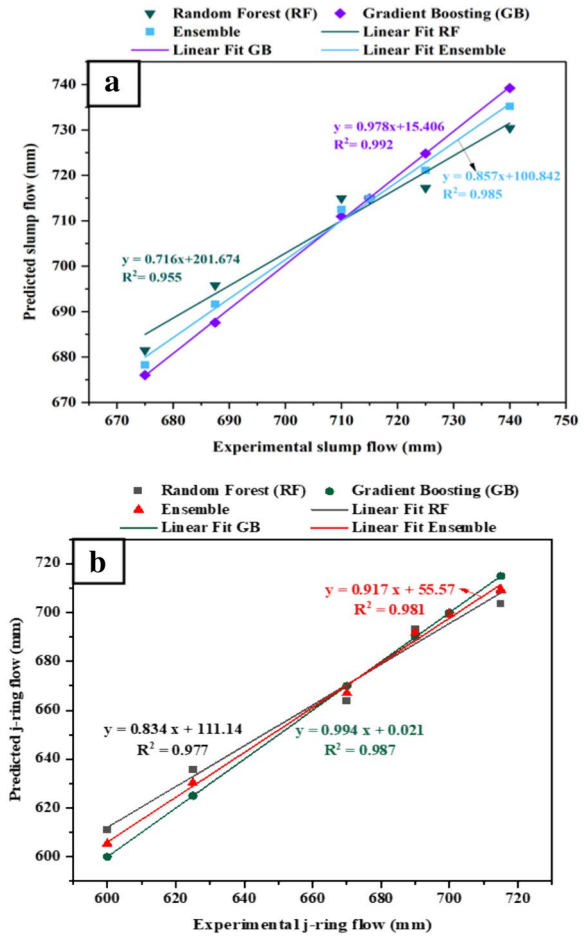

Fig. 5 Correlation between experimental and ML predicted outcomes on (**a**) slump flow and (**b**) J-ring assessment

enhances the accuracy and reliability of concrete quality assessment by allowing for more exact quantification of slump and J-ring flow measurement. By carefully assessing the model's performance, cross-validation, and regularization techniques also aid in avoiding overfitting. Fig. 5a, b represents the outcomes of a regression evaluation done on experimentation data and predictive data of slump flow and j-ring analyses utilizing single-based machine learning algorithms like RF and GB and ensemble models employing this approach. Fig. 5a displays the R^2 values for the RF, GB, and ensemble models applied to estimate the slump flow values, which were 0.955, 0.992, and 0.985 correspondingly, indicating that the prediction results of current models had a satisfactory performance in predicting the respective experimental findings. As a result, these suggested models for slump flow have excellent correlation coefficients. According to Azimi-Pour et al. (2020), large-volume fly ash substitution in SCC resulted in a nearly equivalent coefficient of regression value ($R^2 = 0.974$) in support vector machine (SVM) analysis.

However, Fig. 5b displays the impressive correlation coefficient achieved by the ML-based method when implemented in the prediction of J-ring evaluations. Additionally, most of the data points are clustered along the line of best fit this time around. However, the regression coefficients for the RF, GB, and their ensemble models are all approximately 0.977, 0.987, and 0.981. This means the proposed models have shown the best accuracy with the current investigation.

4.2 Effects of the Hardened Characteristics of HSSCC

4.2.1 Compressive Strength Test

According to different statistical methods, the findings of the compressive strength test are examined in Table 5 in terms of mean strength, standard deviation, coefficient of variation (COV), standard error, and the lower and higher range at a 95% confidence interval. Within a confidence interval of 95% ranging from 30.62 to 32.66 MPa, the minimum compressive strength measured was 31.64 MPa after 7 days of curing. Maximum compressive strength was obtained at 35.17 MPa, with a confidence rate of 95% ranging from 34.71 to 35.64 MPa. The minimum compressive strength seemed 45.21 MPa after 28 days, with 95% confidence varying from 43.33 to 47.09 MPa. A 56-day experiment displayed a minimum amount of compressive strength regarding 46.63 MPa with a confidence rate of 95% ranging from 45.41 to 47.45 MPa. Maximum strength was obtained at 53.57 MPa after 56 days, with a 95% confidence interval of 48.89–58.25 MPa. The COV in the sample data was also rather wide, ranging from 0.81 to 6.31%. The maximum variance was 3.38, and the standard error was 2.39 while assessing compression.

Fig. 6 illustrates the compressive strength and percentages of strength variation among SCC mixtures at 7, 28, and 56 days with changing percentages of MP and constant percentages of SF and FA substitutes. It was demonstrated that the SCC blends with up to 15% MP and constant 10% FA and 20% SF exhibited superior compressive strengths than the control concrete. In several mixes, the greatest compressive strength was obtained when 10% MP, 10% FA, and 20% SF were replaced for SCC. The S20F10M10 mix was observed to have an optimal compressive strength of 35.17 MPa, 50.40 MPa, and 53.57 MPa, superior to reference mixes by 10.39, 10.92, and 14.68% for 7, 28 days, and 56 days, respectively. Better C–S–H gel formation and increased compressive strength are the outcomes of adding MP, which also increases the stiffness and decreases permeability inside the concrete form together with FA and SF. The lowest compressive strength was observed in the

Table 5 Statistical analysis of the compressive strength test outcomes

Mix ID	Curing age (Day)	Mean strength (MPa)	Standard deviation	COV	95% Confidence Level Standard error	Lower bound	Upper bound
S20F0M0	7	31.86	0.3394	0.0107	0.24	31.39	32.33
	28	45.44	0.3677	0.0081	0.26	44.93	45.95
	56	46.71	1.3294	0.0285	0.94	44.87	48.55
S20F10M0	7	32.78	1.3152	0.0401	0.93	30.96	34.60
	28	46.84	1.2304	0.0263	0.87	45.14	48.55
	56	48.75	1.2021	0.0247	0.85	47.08	50.42
S20F10M5	7	34.13	0.4525	0.0133	0.32	33.50	34.76
	28	48.8	1.3859	0.0284	0.98	46.88	50.72
	56	50.62	2.0506	0.0405	1.45	47.78	53.46
S20F10M10	7	35.17	0.3394	0.0097	0.24	34.71	35.64
	28	50.40	1.0182	0.0202	0.72	48.99	51.81
	56	53.57	3.3800	0.0631	2.39	48.89	58.25
S20F10M15	7	32.74	1.8809	0.0575	1.33	30.13	35.35
	28	46.28	1.1172	0.0241	0.79	44.73	47.83
	56	48.42	0.5657	0.0117	0.40	47.64	49.20
S20F10M20	7	31.64	0.7354	0.0232	0.52	30.62	32.66
	28	45.21	1.3576	0.0300	0.96	43.33	47.09
	56	46.43	0.7354	0.0158	0.52	45.41	47.45

S20F10M20 blend, which consisted of 20% MP, 10% FA constant, and 20% SF. Its compressive strength decreased by 0.70, 0.51, and 0.59% at 7, 28, and 56 days, respectively, in comparison to the reference mix (S20F0M0). As MP concentration increases, interparticle contact and homogeneity may reduce, causing reduced strength. According to Khodabakhshian et al. (2018) and Uysal and Yilmaz (2011), its pore-filling influence was responsible for the enhanced compressive strength of mixtures when MP was used to replace cement up to 10%.

4.2.1.1 Predictive Performance of Bagging and Boosting ML Algorithms on Compression When utilizing ML techniques, such as random forest, gradient boosting, and their ensemble models to estimate concrete compressive strength from a dataset containing 230 experimental and literature review samples, each data point contains specific characteristics representing the composition of the concrete mixture as well as the corresponding strength measurement. The aforementioned characteristics include numerical values for a range of constituent substances, including fine aggregate, coarse aggregate, cement, water, and possible admixtures incorporated into the concrete composition. Further, qualitative variables are frequently incorporated as supplementary characteristics, including curing conditions, the age of the concrete at the time of testing, and the environmental conditions that were prevalent during the testing process. Every data point in the dataset reflects a unique mix of these attributes as well as the measured concrete compressive strength, which serves as the target variable for the ML models. ML algorithms analyze these data points in great detail, finding complex relationships between the input variables and concrete strength. Fig. 7 depicts the boxplots of the experimental and predicted correlation. Mean and standard deviation are shown, along with other statistical measures, such as median, interquartile range, minimum, and maximum. The methods are assessed and contrasted to determine the best prediction strategy that generates enhanced outcomes with excellent accuracy. The results revealed that the distribution of the predicted and experimental outcomes for no model was significantly skewed. All median lines were within their respective boxes, suggesting that there was likely no distinction across the datasets. Furthermore, no outliers were identified in either the RF or GB models.

Fig. 8 illustrates that the RF and GB approaches provide accurate predictions when contrasted with the experimental outcomes and literature review datasets. Although it provides valuable insights, the established correlation between concrete properties and predictive models has deficiencies. These include possible discrepancies in forecasting precision due to dataset qualities, issues associated with overfitting, difficulties in capturing all the variables of concrete behavior, lack of generalization to diverse situations, and the requirement for

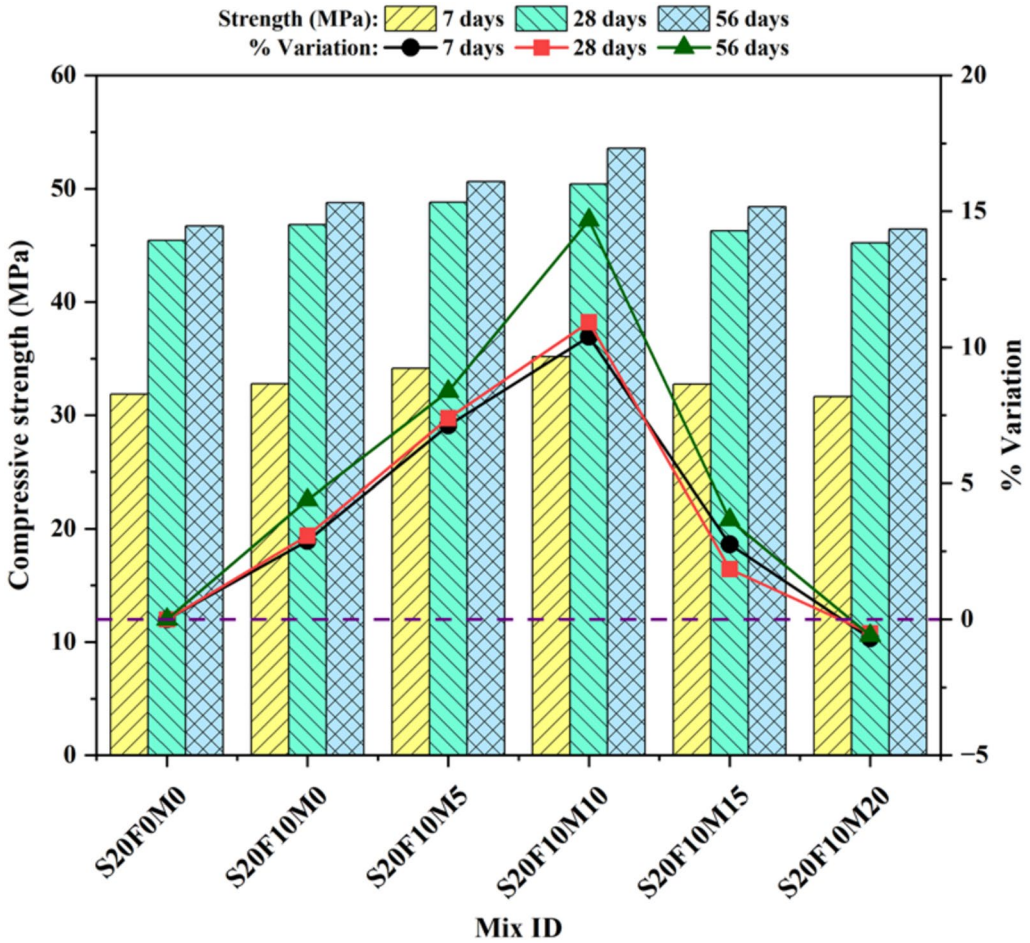

Fig. 6 Hardened properties of compressive strength test and the variation of percentage on HSSCC mixtures

cautious validation and interpretation of outcomes due to inherent biases in ML techniques. To attain precise predictions while preventing overfitting, it is imperative to conduct thorough preprocessing of the dataset, which encompasses addressing missing data and normalizing features. By dividing the dataset into training and testing sets, precise model evaluation is facilitated, with the assistance of cross-validation methods. Consistently evaluating the performance of the model and adjusting hyperparameters are essential to derive precise predictions from the dataset without inadvertently overfitting. In the RF and GB models, the correlation coefficient was 0.93 and 0.97, respectively, while ensemble models generated a value of 0.94. However, it is clear from the prediction graph, where the values are clustered along the prediction line, that the predicted outcomes for the model run with GB were rather close to the actual statistics. Using bagging analysis, Azimi-Pour et al. (2020) found that substituting significant amounts of SCC with fly ash had a pretty comparable coefficient of regression value.

From Table 6, it is clear that the GB model has a much higher R^2 value compared to the RF and ensemble model. As a result, it may be inferred that the GB model is highly predictive. In terms of MAE, MSE, and RMSE the GB model performed the most effectively, with values of 1.76, 4.87, and 2.21, respectively.

4.2.2 Splitting Tensile Strength Test

Table 7 reflects the splitting strength results of the various MP proportions combined with a constant percentage of FA and SF components throughout all SCC samples, based on statistical evaluations such as compressive strength tests. The findings of the samples' deviation ranged from 0.0424 to 0.495, with a COV of 0.84–11.22% and a standard error of 0.03–0.35.

Fig. 9 illustrates the outcomes of tensile strength splitting and percentage variation off SCC mixtures with the

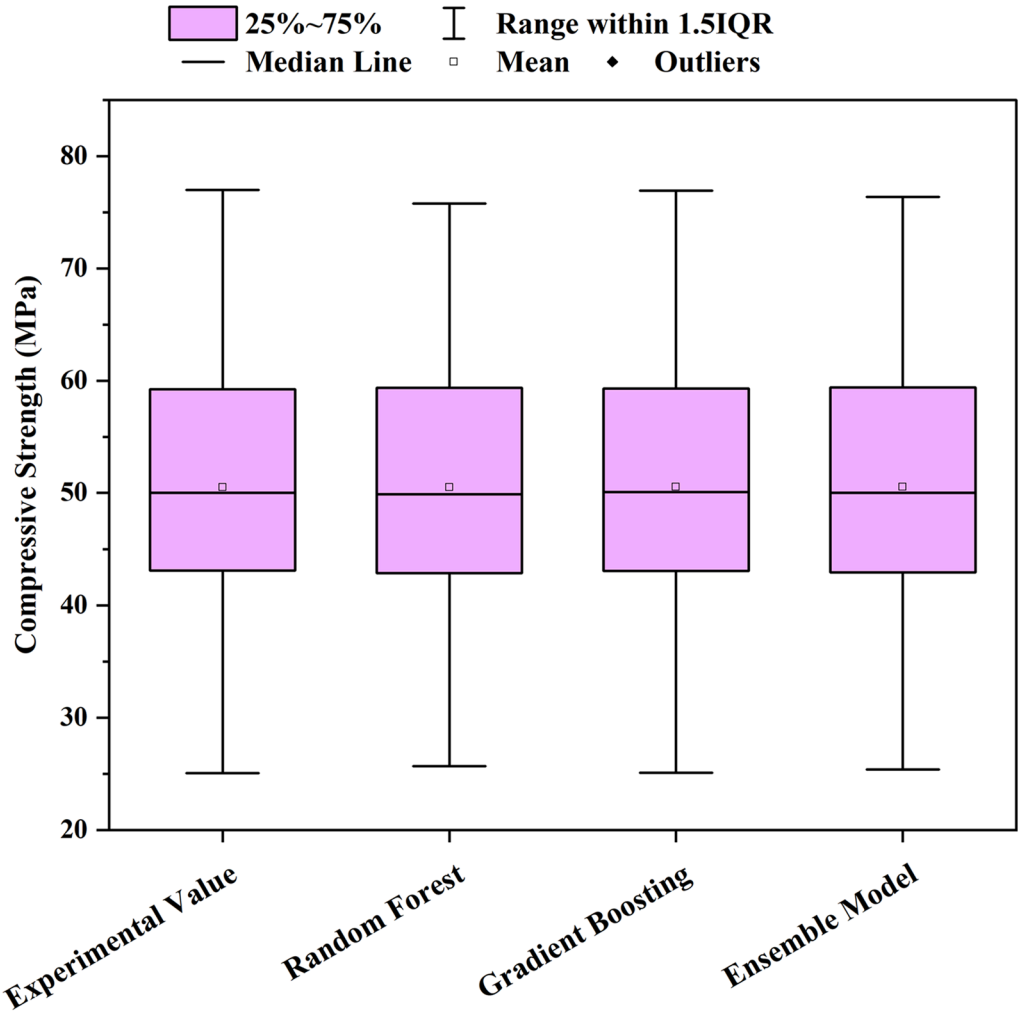

Fig. 7 Box plot exhibiting the data distribution for compressive strength with machine learning algorithms

addition of MP, FA, and SF integration during the curing ages of 7, 28, and 56 days. The progression of splitting tensile strength seems comparable to the pattern of compressive strength, where strength decreases as the MP percentage increases. Nevertheless, replacing cement with MP combined with constant FA and SF typically increased splitting tensile strength by up to 15% in contrast to the reference mixture. As shown, this cementitious material decreases strength when used excessively. S20F10M20 had 17.32, 15.19, and 15.59% greater splitting tensile strengths than the control mix at 7, 28, and 56 days. As a result of lessening the concrete's porosity and increasing its packing densities, MP can increase the overall splitting tensile strength of the concrete. The S20F10M20 mix displayed the lowest splitting tensile strength, with declines of 2.36, 2.27, and 6.62% in the curing times of 7, 28, and 56 days in comparison to the reference mixture. This is because a higher concentration of MP results in more pore space and weaker interparticle bonds, all of which have lower strength. Khodabakhshian et al. (2018) in TVC and Sharma and Khan (2017b) in SCC revealed nearly parallel test outcomes. Comparable to the current investigation, Ali et al. (2022) found that combining polypropylene fibers with marble powder in SCC increased the split tensile strength by 16.92%.

4.2.2.1 Predictive Performance of Bagging and Boosting ML Algorithms on Tension In employing ML methods like RF, GB, and ensemble models to forecast the splitting tensile strength of concrete from a dataset comprising 230 experimental and literature review datasets, each data point encapsulates distinct attributes reflecting the composition of the concrete mixture and the associated splitting tensile strength measurement. Each experimental sample in the dataset has a different mix of these characteristics in addition to the measured concrete splitting

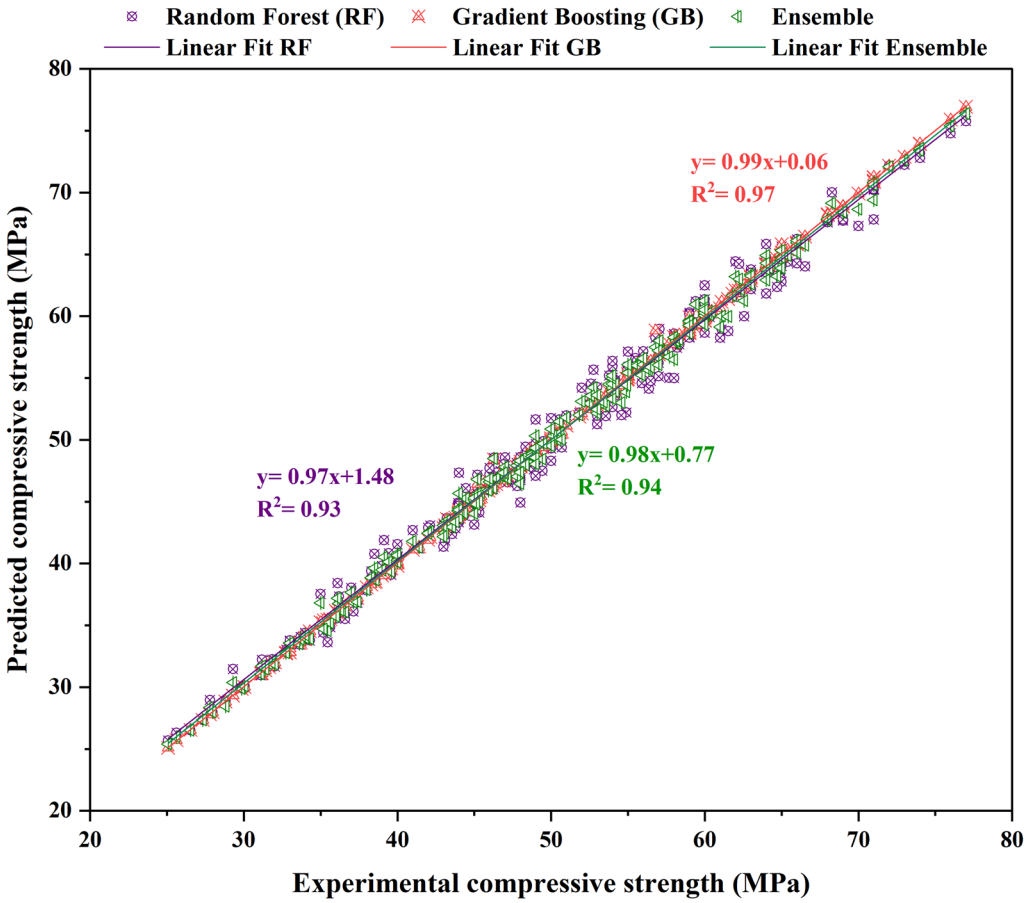

Fig. 8 Correlation between experimental and predicted compressive strength outcomes of bagging and boosting models

Table 6 Performance criteria of the developed bagging and boosting methods

Criteria	RF	GB	Ensemble
R^2	0.93	0.97	0.94
MAE	2.36	1.76	1.98
MSE	8.95	4.87	5.51
RMSE	2.99	2.21	2.37

tensile strength, which is used as the dependent variable in ML models. Boxplot representations of the experimental and predicted results are presented in Fig. 10. None of the models had extremely erroneous distributions of predicted and experimental findings. Since each median line was located inside its box, this implies that there most likely was no significant difference between the datasets. Both the RF and GB models did not reveal any outliers.

Fig. 11 reveals that compared to experimental results, both the RF and GB methods seem to produce suited predictions. Potential discrepancies in forecasts caused by the quality of the dataset, concerns about overfitting, restricted applicability, and the necessity for careful validation owing to inherent biases in machine learning are all limitations of the correlation between concrete properties and predictive models. For accurate predictions that prevent overfitting, it is vital to perform exhaustive preprocessing of the dataset, which includes restoring features and addressing missing data. With the use of cross-validation methods, separating the dataset into a training set and a testing set allows for a more accurate model assessment. Predicted results for the model conducted with GB were very close to the actual outcomes, as seen by the prediction graph, in which the values are organized near the prediction line. de-Prado-Gil et al. (2022) observed that the correlation coefficient of the regression analysis value of the SCC generated with recycled aggregates had a highly comparable value when applying extreme gradient boosting (XG Boost).

Table 8 demonstrates that the GB model outperforms the RF and ensemble models regarding R^2 value. This suggests that the GB approach has a significant level of predictive ability. The GB model fared the best, with

Table 7 Statistical analysis of the splitting tensile strength test outcomes

Mix ID	Curing age (Day)	Mean strength (MPa)	Standard deviation	COV	95% Confidence Level Standard error	Lower bound	Upper bound
S20F0M0	7	3.81	0.3394	0.0891	0.24	3.34	4.28
	28	4.41	0.4950	0.1122	0.35	3.72	5.09
	56	4.68	0.1980	0.0423	0.14	4.41	4.95
S20F10M0	7	4.06	0.1556	0.0383	0.11	3.84	4.28
	28	4.68	0.1697	0.0363	0.12	4.45	4.92
	56	4.8	0.0990	0.0206	0.07	4.66	4.94
S20F10M5	7	4.24	0.2404	0.0567	0.17	3.91	4.57
	28	4.81	0.0849	0.0176	0.06	4.69	4.93
	56	5.30	0.1838	0.0347	0.13	5.05	5.56
S20F10M10	7	4.47	0.1980	0.0443	0.14	4.19	4.74
	28	5.08	0.2970	0.0585	0.21	4.67	5.49
	56	5.41	0.1980	0.0366	0.14	5.14	5.68
S20F10M15	7	3.97	0.2828	0.0713	0.20	3.58	4.36
	28	4.61	0.2970	0.0644	0.21	4.20	5.02
	56	5.04	0.0424	0.0084	0.03	4.98	5.09
S20F10M20	7	3.72	0.0566	0.0152	0.04	3.63	3.80
	28	4.31	0.3677	0.0853	0.26	3.80	4.82
	56	4.37	0.1414	0.0324	0.10	4.17	4.57

values of 0.21, 0.08, and 0.29 for MAE, MSE, and RMSE. The algorithms of the GB framework are responsible for its exceptional performance.

4.3 Effects of the Durability Characteristics of HSSCC

4.3.1 Water Permeability Test

The water penetration depth of several concrete specimens is illustrated in Fig. 12 after 56 days of the curing age. The specimen with 10% MP, 10% FA, and 20% SF had the lowest water penetration depth of all the mixtures at approximately 14 mm, with a decrease of 39.13% from the control mixture. As a result, the water permeability might vary depending on the SF, FA, and MP combination. Including MP significantly lowers the water penetration depth by up to 15% of the replacement. The addition of MP, FA, and SF to concrete enhanced packing density, which improved durability by filling internal voids between fine aggregates and decreased water penetration depth. The assessment made after water is continuously circulated through concrete specimens of MP for 72 h is satisfactory for construction activities in high-humidity, moist, or high-atmospheric-pressure regions. Gesoğlu et al. (2009) noticed that the quaternary blend of SF, FA, and blast furnace slag (BFS), as well as the binary cement containing SF, had the lowest water penetration depths in SCC compared to the control mixture, thus being nearly the same as this proceeding research. The possibility of a water retention access may cause several kinds of durability concerns, such as freeze–thaw damage, corrosion of structural strengthening, and chemical violence is minimized when the depth of water penetration is kept lower than 25 mm. Due to the depth of water penetration having to exceed 25 mm during the permeability test, it is concluded that the specimens have become weakened (Chung et al., 2013).

4.3.2 Sorptivity Test

The findings of the water absorption of the HSSCC at 56 days of curing are shown in Fig. 13. Nearly identical patterns could be observed in all sorptivity test outcomes. After 56 days, adding MP, FA, and SF drastically lowered the absorption rate. The S20F10M20 mixture had a maximum water sorptivity over the 56-day curing period. In a sorptivity test, adding MP to SCC mixes at 5% and 10%, along with consistent amounts of 20% SF and 10% FA, reduced water absorption by 3.57% and 14.29%, respectively; however, it enhanced 14.28% and 42.85% when 15% and 20% MP were incorporated, compared to the control mix. HSSCC likely had better durability in the sorptivity test than any other SCC mixes due to using 10% MP, constant 10% FA, and 20% SF. The incorporation of this SCM reduces the sorptivity coefficient, which in turn causes the concrete to absorb less water, resulting in increased resistance to water penetration and improved durability. Furthermore, incorporating MP in higher concentrations improves concrete porosity, allowing

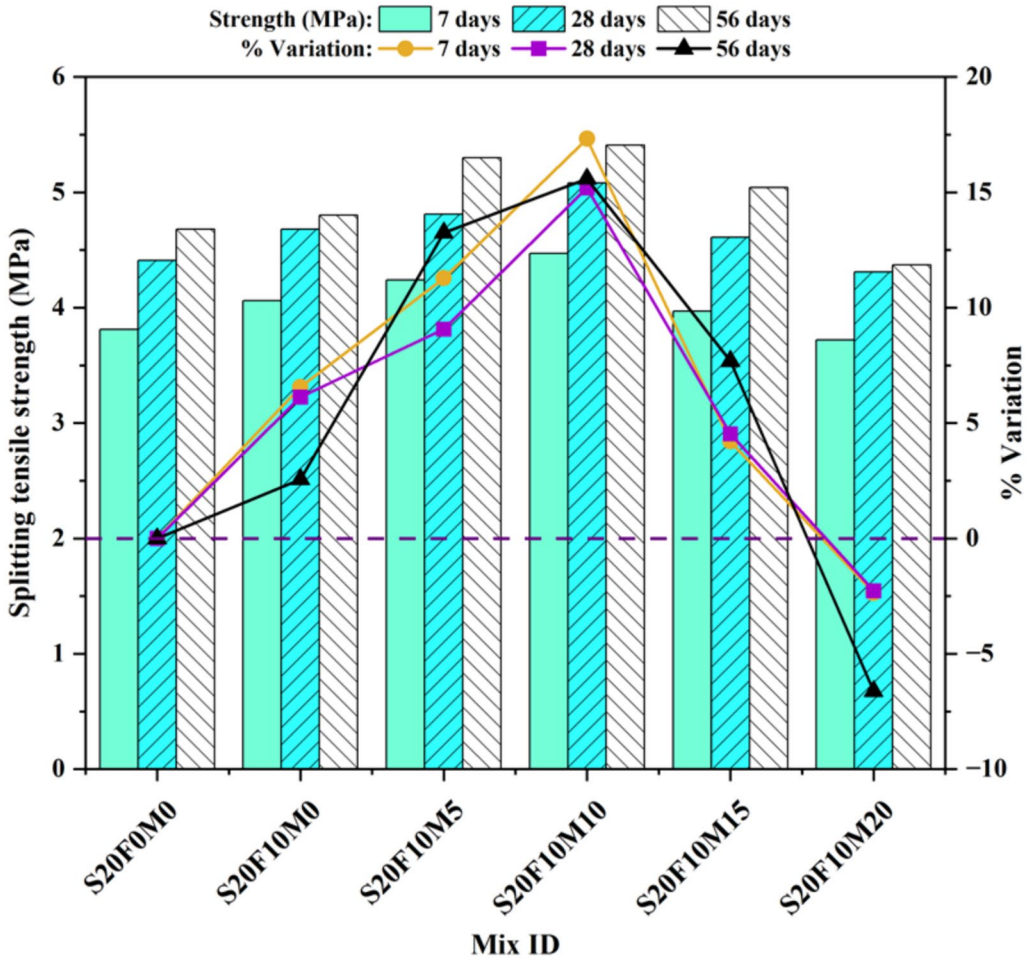

Fig. 9 Hardened properties of splitting tensile strength test and the variation of percentage on HSSCC mixtures

additional paths for water to penetrate and enhancing the sorptivity coefficient. Sharma and Khan (2017a) observed that SCC incorporating copper slag exhibited a substantial decrease in water absorption, with sorptivity readings reduced by up to 60%, resulting in significantly enhanced impermeability compared to this study's results. According to Md (2019), steel fiber-reinforced SCC (SFRSCC) cumulative water absorption increased as time progressed and also displayed equivalent results compared to this investigation.

4.3.3 Rapid Chloride Penetration Test (RCPT)

Fig. 14 illustrates the findings of chloride penetration tests for all SCC combinations regarding the amount of total charge passed after curing for 56 days. The investigation found that incorporating 0–15% MP along with steady amounts of 10% and 20% FA and SF in the SCC mixture led to a decrease in chloride penetration, in contrast to incorporating 20% MP in addition to the same amounts FA and SF, which increased chloride penetration in comparison with the control mix. The RCPT values reduced by 5.75, 22.41, 37.36, and 20.69% when MP was replaced at 0, 5, 10, and 15% together with a constant 10% FA and 20% SF, whereas MP at 20% replacement indicated an increase of 2.30% instead of the control mixture. The pozzolanic activity of these substances may enhance the durability of concrete by causing the formation of additional C–S–H as well as the generation of pores in the concrete matrix. On the contrary, a higher concentration of MP may also accelerate the production of additional reaction products, making it easier for chloride ions to circulate and enhance the RCPT values. The graph demonstrates that the mix S20F10M10 had the lowest charge travelling through it at 981 Coulombs, exhibiting that it was more durable than other SCC mixtures. Following the ASTM C1202 standards, the passing charges were low to very low, which might further reduce the concrete's porosity (ASTM-C, 1202, 2019). Givi et al. (2010) stated that the high concentration of SiO_2 in rice husk ash (RHA) established an extremely reactive

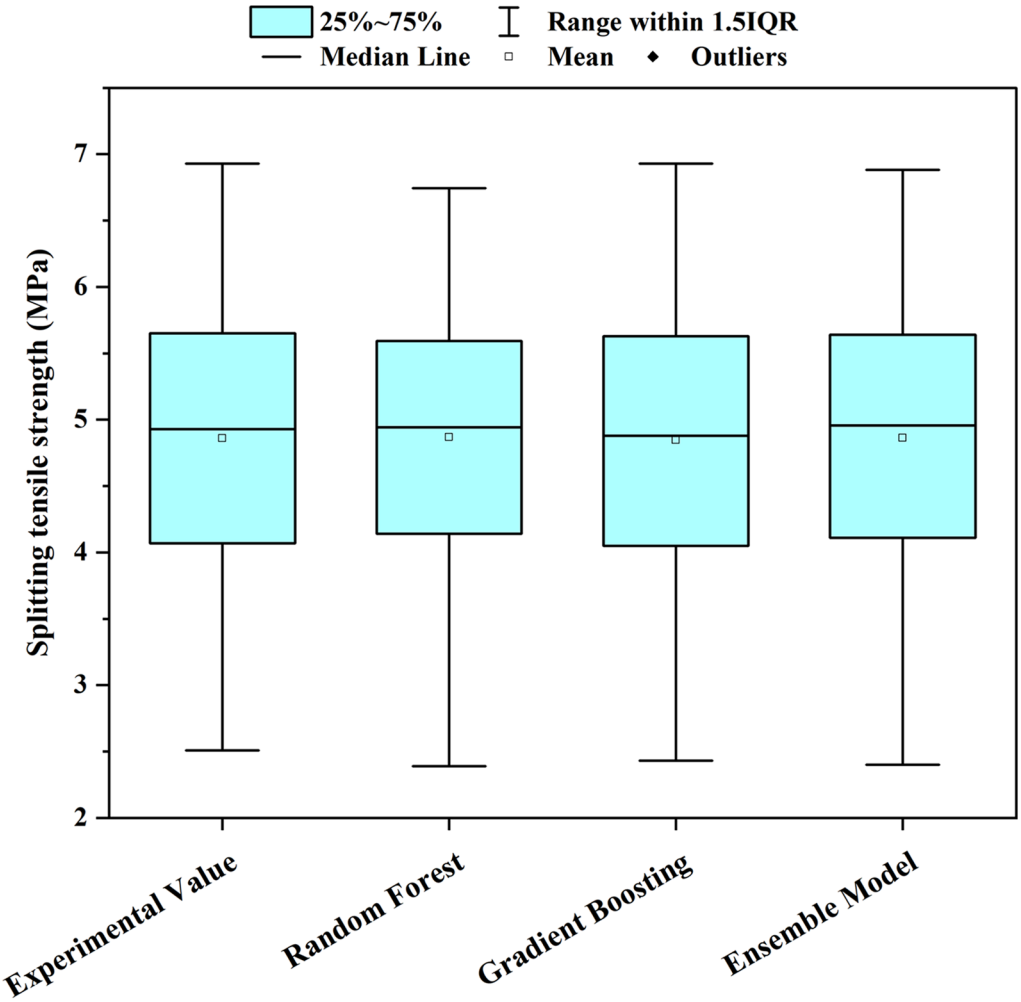

Fig. 10 Box plot exhibiting the data distribution for splitting tensile strength with machine learning algorithms

pozzolanic substance used to formulate more C–S–H gel, enhancing concrete formation.

4.4 Effects of the Non-Destructive (NDT) Characteristics of HSSCC

4.4.1 Rebound Hammer Test

The statistical outcomes of the digital rebound hammer assessment analysis are summarized in Table 9, where the mean rebound number (RN) was found to vary from 22.66 to 32.20. With a COV that ranged from 0.0108 to 0.0458, the standard deviation for all values fluctuated between 0.3253 and 1.1314.

The mean rebound number (RN), which was determined through analysis of digital rebound hammer assessment, can be depicted in Fig. 15. The test was performed on a specimen curing for 28 and 56 days. The SCC surface layer is regarded as a "good layer" up to a 15% substitution of the MP, coupled with a constant 10% FA and 20% SF, respectively. Despite the porosity of the ITZ within the concrete samples, it can be observed that the RN value of the control was lower than that of all other SCC mixes except the S20F10M20 mix. The S20F10M10 mix had the greatest RN at 28 days, which is 31.9, and at 56 days, which is 32.2, whereas the S20F10M20 mix had the lowest RN at 22.6 and 26.3 at the curing times of 28 days and 56 days, respectively as compared to the reference mix. According to Singh et al. (2017), the outcomes of this experiment were extremely comparable with the findings of the rebound hammer test of waste marble powder substitutes.

4.4.2 Ultrasonic Pulse Velocity (UPV) Test

The statistical results for flexural strength for SCC specimens containing different MP content percentages and consistent percentages of FA and SF are exhibited in Table 10. With a COV between 0.00429 and 0.01692, the standard deviation for UPV values encompassed 19.799 to 70.711.

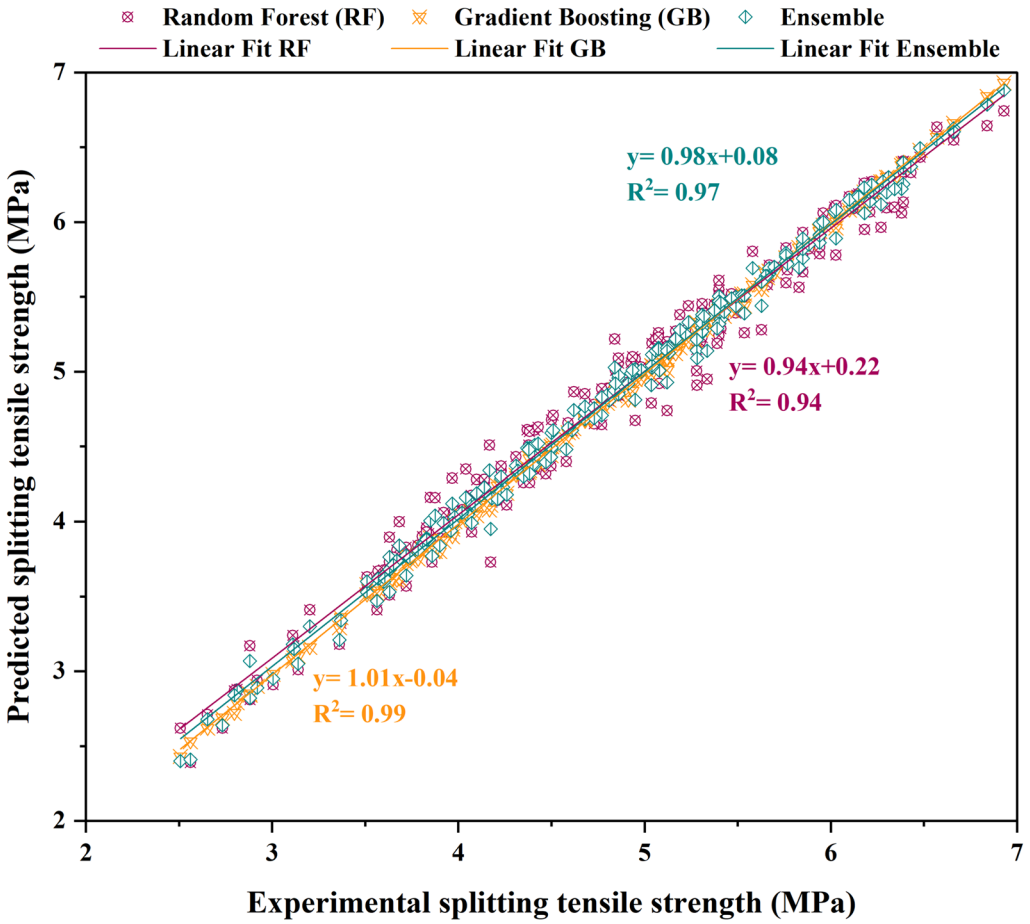

Fig. 11 Correlation between experimental and predicted splitting tensile strength outcomes of bagging and boosting models

Table 8 Performance criteria of the developed bagging and boosting methods

Criteria	RF	GB	Ensemble
R^2	0.94	0.99	0.97
MAE	0.23	0.21	0.22
MSE	0.11	0.08	0.10
RMSE	0.34	0.29	0.31

As depicted in Fig. 16, the specimen underwent UPV testing at 28 and 56 days with varying MP percentages alongside consistent FA and SF percentages. In comparison, the variable concentration of MP alongside the constant concentration of FA and SF exhibited UPV values fluctuating between 4136 and 4929 m/sec at 28, and 56 days. A control mix, S20F0M0, demonstrated an impressive UPV value of 4065 m/sec after 28 days and 4580 m/sec after 56 days, indicating that pulse velocity enhances with the duration of more curing ages and enhances the grading quality of concrete "excellent" following ASTM C597 criteria (Astm). The optimum UPV value was noticed in the S20F10M10 mix, whereas the pulse velocity was 4285 m/sec and 4929 m/sec for the curing periods of 28 and 56 days, respectively. In contrast to the control mix, the pulse velocity values in a mixture including 5–20% replacements of MP along with constant 10% FA and 20% SF increased by 0.65, 5.61, 7.62, 6.70, and 2.21% during the 56-day curing period. As a result, such an investigation demonstrated that a higher proportion of replacement resulted in a denser structure and enhanced concrete density, resulting in a higher pulse velocity. Uysal and Yilmaz (2011) reported an equivalent outcome using marble slurry powder (MSP). According to their findings, MSP using up to 10% enhanced UPV values, whereas higher MSP substitution with cement caused lower UPV values. Uysal and Sumer (2011) also found comparable outcomes with nearly equivalent pulse velocities achieved by incorporating FA into SCC mixtures as a 25% cement replacement.

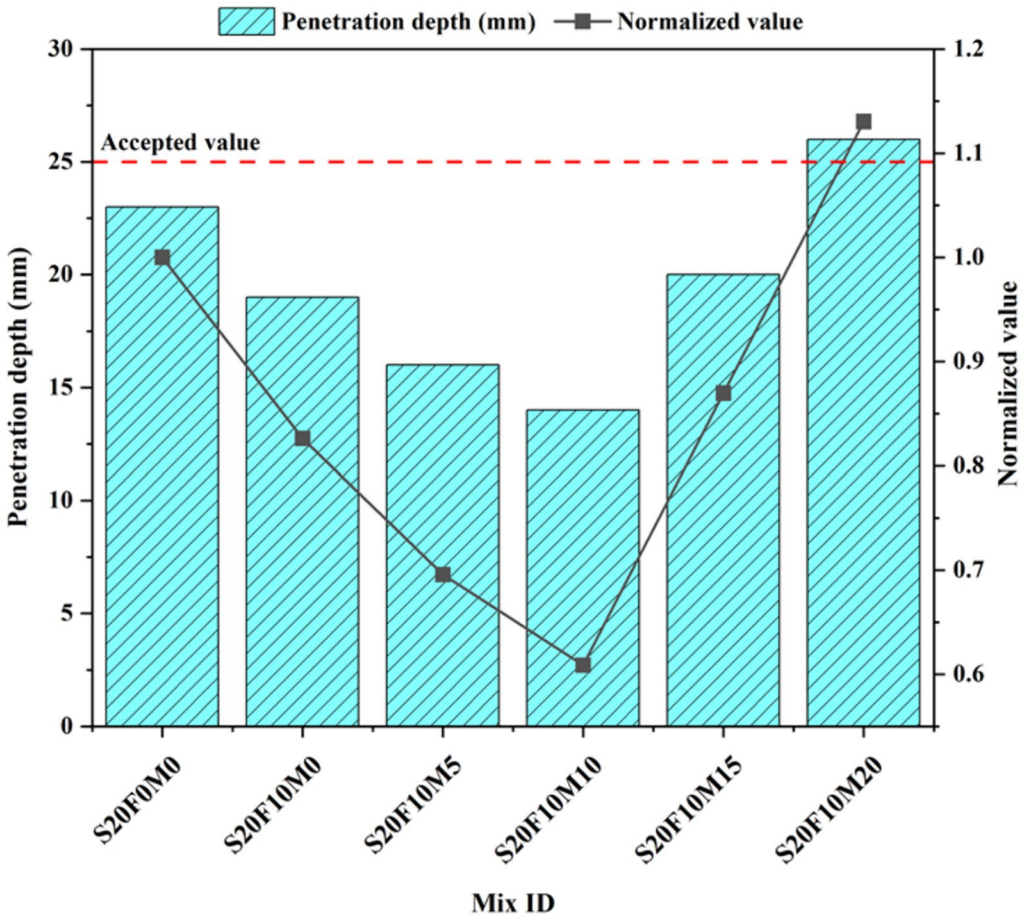

Fig. 12 Water penetration depth of the HSSCC mixtures

4.5 Relationship between DT and NDT Properties of HSSCC

4.5.1 Compressive Strength Versus Rebound Number (RN)

This investigation additionally recommends one variable in the equation for regression for determining the compressive strength of concrete according to several regression analyses. The correlation associated with compressive strength (f'c) and rebound number (RN) can be illustrated in Fig. 17. A modest percentage of variability and high stability of the findings can be observed by the coefficient of regression (R^2) value, which is approximately 82.67%. The graphical representations of the points were acquired from multiple investigations on rebound number and compressive strength from Sunayana and Barai (2017), Datta et al. (2022), Domingo and Hirose (2009), Singh et al. (2017), and De Almeida (1991). The association with the destructive strength and rebound number value of the SCC specimens, which include varying percentages of MP alongside consistent percentages of FA and SF, is likewise expressed in this equation. Furthermore, the predicted interval and 95% confidence interval function are determined to illustrate the observed relations precisely. Nevertheless, because of varying mixes of concrete, Sunayana and Barai (2017), Datta et al. (2022), Domingo and Hirose (2009), and Singh et al. (2017) displayed variations beyond the confidence interval of 95% level region. According to the findings of De Almeida (1991) and the outcomes of this investigation, the expected compressive strength deviates by an average of almost 3%.

4.5.2 Compressive Strength Versus Ultrasonic Pulse Velocity (UPV)

The correlation between the compressive strength and UPV of each combination is represented in Fig. 18. Relatively poor results can be observed by the coefficient of regression (R^2) value, which is about 78.73%. The dispersion of every data series from the typical trend line is highlighted. The substitution of varying MP percentages was mainly responsible for the dispersion of the data points. In this scenario, the parameters impacting validations tend to be so bound that it might be complicated to accomplish a confidence level of 95% intervals higher

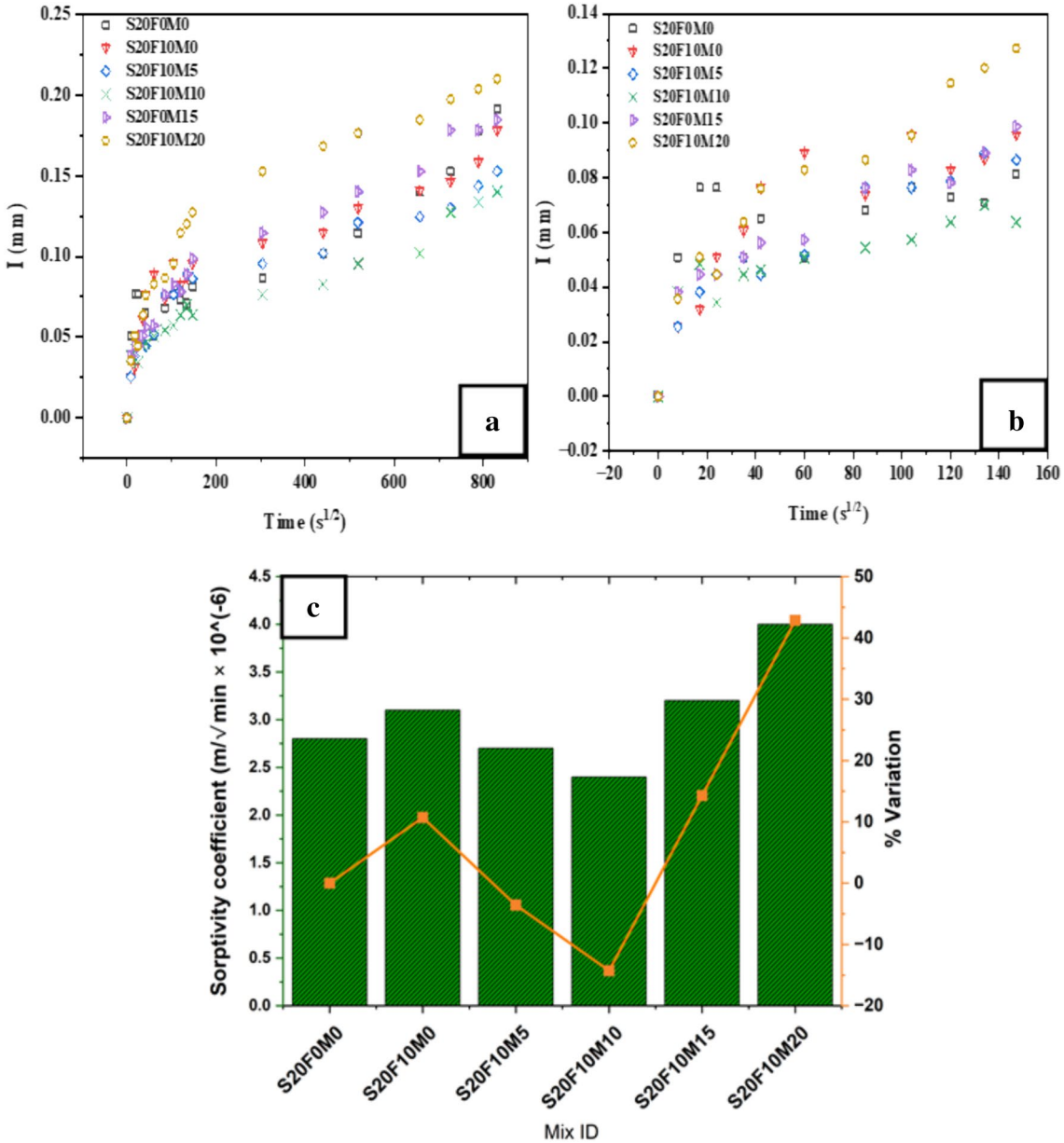

Fig. 13 Sorptivity test of the HSSCC mixtures on (**a**) capillary absorption (**b**) initial absorption and (**c**) summarized coefficients at 56 days

than 20% during precise strength anticipation of in situ concrete, regardless of optimal circumstances and a particular validation (Madandoust et al., 2010). The graphical points were extracted through multiple studies on UPV and compressive strength by Belagraa et al. (2015), Sunayana and Barai (2017), Vo et al. (2021), Datta et al. (2022), and Singh et al. (2017). However, Datta et al. (2022), and Vo et al. (2021) exhibit variations beyond the 95% confidence level region as an outcome of multiple concrete mixtures. The analyses carried out by Singh et al. (2017) and the present investigation revealed differences by an average of almost 19.03%. On the contrary, this investigation and the findings of Belagraa et al. (2015) demonstrated a nearly 4% average divergence from the expected compressive strength.

4.6 Effects of the Microstructural Characteristics of HSSCC

Fig. 19a–d displays SEM micrographs of certain HSSCC mixtures whereas Fig. 19a illustrates the surface morphology of the control mixture. The control mix has noticeable surface fractures and poor interfacial transition zone (ITZ). As opposed to the control

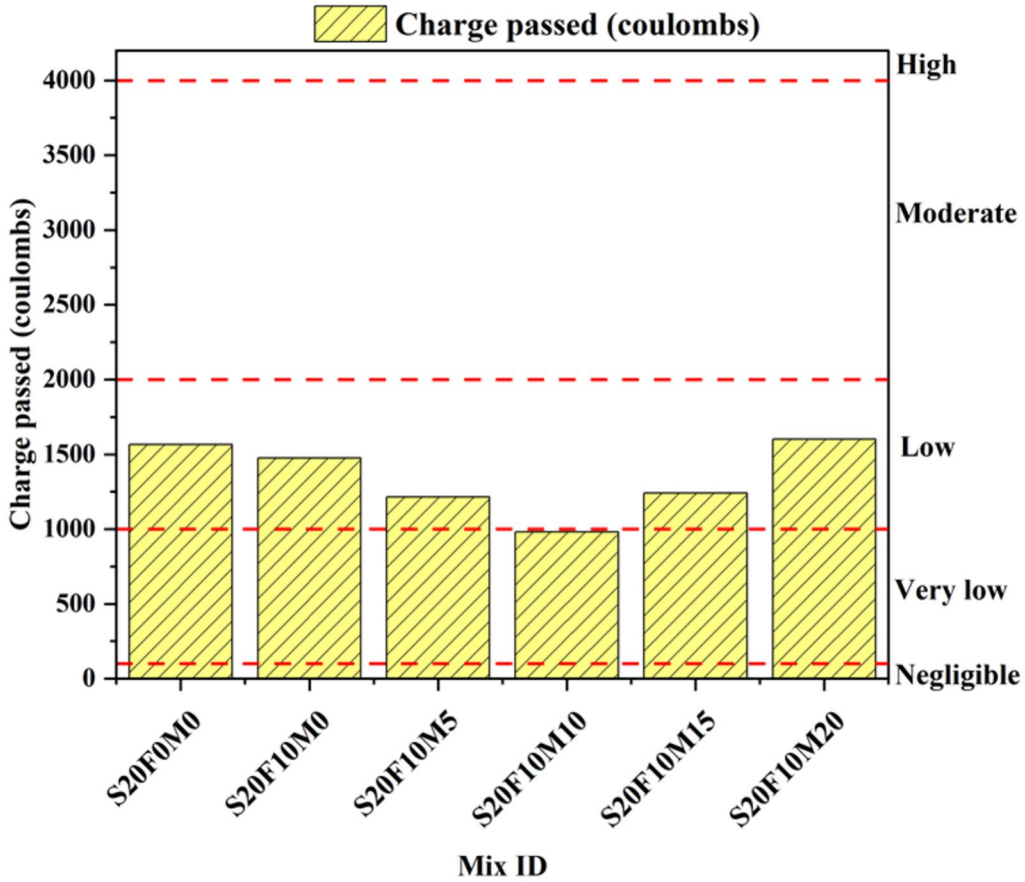

Fig. 14 RCPT test of the HSSCC mixture

Table 9 Statistical analysis of the rebound number test results

Mix ID	Curing age (Day)	Mean RN	Standard deviation	COV	95% Confidence Level Standard error	Lower bound	Upper bound
S20F0M0	28	24.7	1.1314	0.0458	0.80	23.132	26.268
	56	27.7	0.8910	0.0321	0.63	26.465	28.935
S20F10M0	28	27.1	0.9051	0.0334	0.64	25.846	28.354
	56	30.1	0.3253	0.0108	0.23	29.649	30.551
S20F10M5	28	29.3	0.4667	0.0159	0.33	28.653	29.947
	56	32.1	1.3011	0.0405	0.92	30.297	33.903
S20F10M10	28	31.9	0.3818	0.0119	0.27	31.371	32.429
	56	32.2	0.7212	0.0224	0.51	31.200	33.200
S20F10M15	28	26.7	0.8910	0.0333	0.63	25.465	27.935
	56	30.1	0.3818	0.0126	0.27	29.671	30.729
S20F10M20	28	22.6	0.9192	0.0406	0.65	21.326	23.874
	56	26.3	0.9758	0.0371	0.69	24.948	27.652

mixture, the HSSCC mixture having MP, SF, and FA had enhanced ITZ and a narrower crack width, indicating better mechanical performance. Fig. 19b illustrates an observation of micropores on the surface of the S20F10M0 mixture. SEM micrographs of HSSCC mixtures containing MP revealed a higher ITZ and the

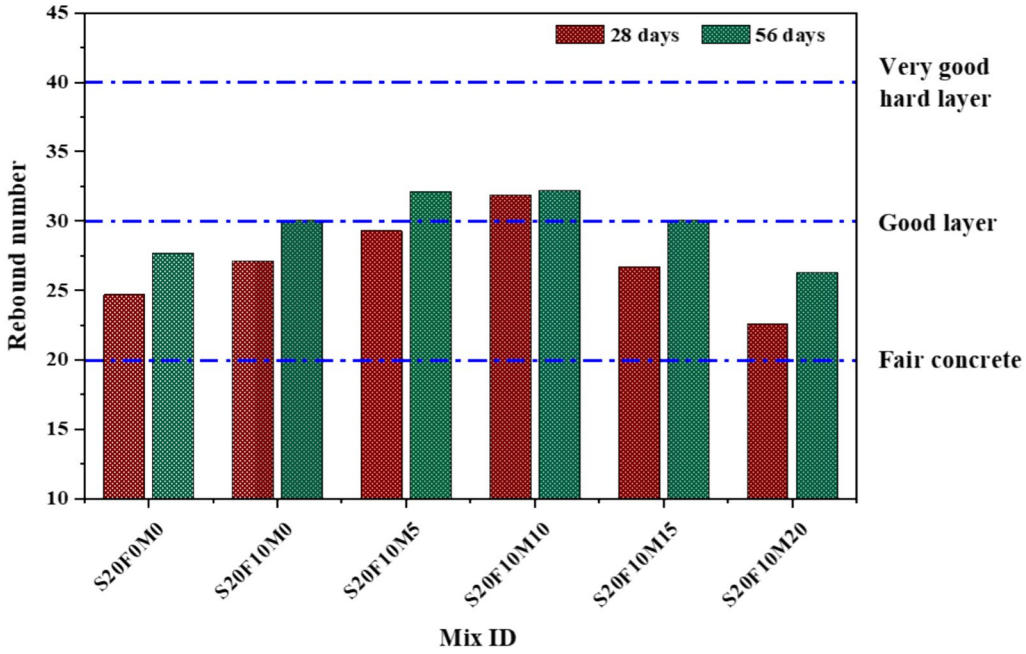

Fig. 15 Rebound hammer test of HSSCC specimens

Table 10 Statistical analysis of the UPV test results

Mix ID	Curing age (Day)	Mean UPV (m/sec)	Standard deviation	COV	95% Confidence Level Standard error	Lower bound	Upper bound
S20F0M0	28	4065	21.213	0.00522	15	4035.60	4094.39
	56	4580	56.569	0.01235	40	4501.60	4658.39
S20F10M0	28	4207	28.284	0.00672	20	4167.80	4246.19
	56	4610	19.799	0.00429	14	4582.56	4637.43
S20F10M5	28	4236	56.569	0.01335	40	4157.60	4314.39
	56	4837	28.284	0.00585	20	4797.80	4876.19
S20F10M10	28	4285	28.284	0.00660	20	4245.80	4324.19
	56	4929	45.255	0.00918	32	4866.28	4991.71
S20F10M15	28	4178	70.711	0.01692	50	4080.00	4275.99
	56	4887	22.627	0.00463	16	4855.64	4918.35
S20F10M20	28	4136	22.627	0.00547	16	4104.64	4167.35
	56	4681	35.355	0.00755	25	4632.00	4729.99

absence of any observable crack. However, mechanical performance declined as a consequence of OPC dilution caused by increased MP substitution. HSSCC mix S20F10M10 exhibited outstanding surface morphology, which is apparent in Fig. 19c. The superior mechanical performance may be attributed to the compact concrete matrix with fewer pores in the HSSCC mix consisting of 10% MP, 20% SF, and 10% FA. Fig. 19d displays the SEM micrograph of mix S20F10M20. In this micrograph, reduced ITZ and minimal visible fractures were observed, with the S20F10M20 combination appearing to exhibit an even more porous and less dense structure compared to other HSSCC combinations. Singh et al. (2017) observed findings for MP substitution that were pretty comparable to the findings of the present investigation.

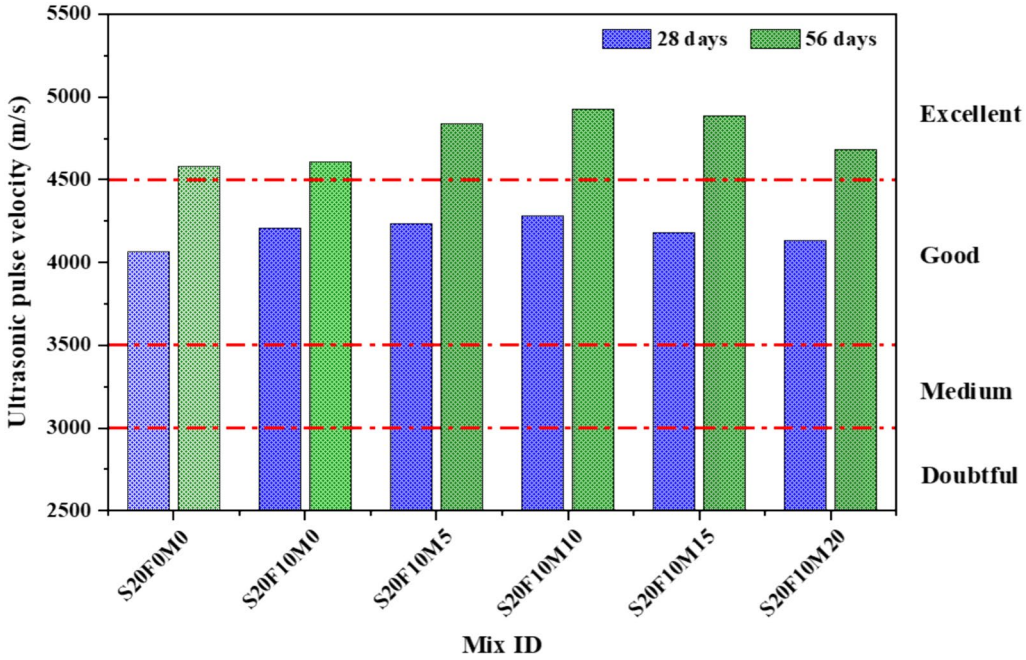

Fig. 16 UPV test of HSSCC specimens

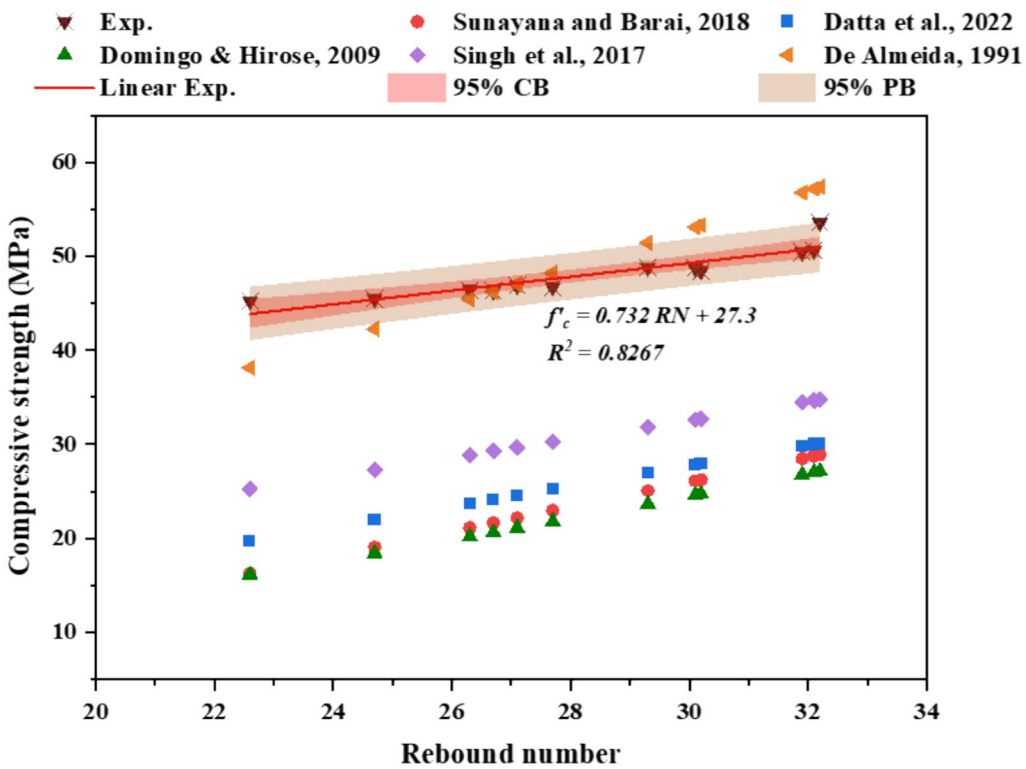

Fig. 17 Correlation between the compressive strength and rebound number of HSSCC

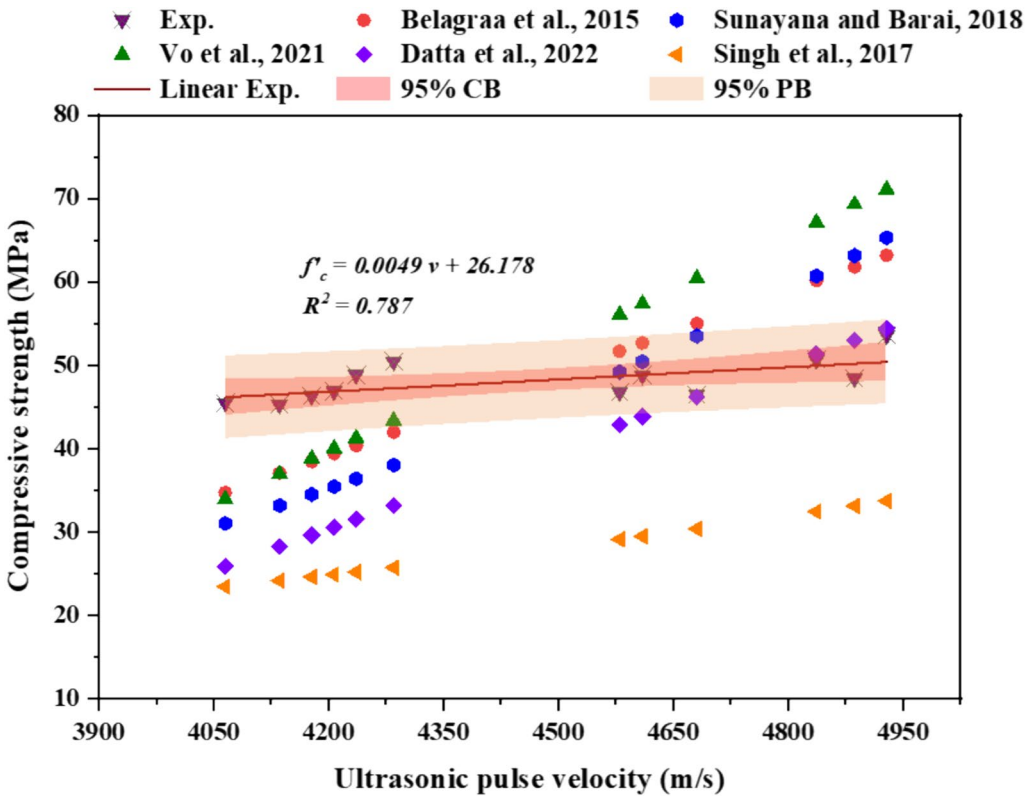

Fig. 18 Correlation between the compressive strength and UPV of HSSCC

4.7 Environmental Impact Evaluation

OPC generates from 75 to 90% of the global CO_2 emission that concrete produces since it is the main binder component of concrete (Khair et al., 2024; Rahman et al., 2022). Alternative binders have been developed to lessen the dependency on OPC due to rising concerns about its potential for worldwide warming (kg CO_2-eq/kg material). Although using SCMs reduces the overall embedded greenhouse gas (GHG) emissions of building materials, the embedded GHG of various types of waste differs (S. Rahman et al., 2023a, 2023b). MP, SF, and FA were partly used as binding agents alternative to OPC for the current investigation. This research assesses the entire emissions of CO_2, taking into account the comparable CO_2 exposures for every material to emphasize the implications of FA, MP, and SF upon the entire embodied GHG emissions. Table 11 compiles the carbon content embodied data for every mixture of concrete after analyzing the emissions of CO_2 of every ingredient per $1m^3$ of concrete and summing those numbers together employing Eq. (5).

$$CO_{2Concrete} = \sum_{i=1}^{n} (CO_{2i-e} \times W_i) \quad (5)$$

Fig. 20 reveals that overall CO_2 emissions were lowered when OPC was partially replaced with different percentages of MP alongside a steady percentage of FA and SF. The control concrete S20F0M0 mixture produced 455.90 kg CO_2/m^3 using a more significant cement proportion. Cement produces roughly 89% embodied carbon. As contrasted with the reference mixture, the total amount of carbon embodied dropped by 10.67, 15.68, 20.69, 25.70, and 30.70% when OPC partially substituted MP at 0, 5, 10, 15, and 20% with a constant proportion of 20% SF and 10% FA. Despite the environmental benefits, the significant reduction in compressive strength resulted from greater use of MP and mineral admixtures. In such a scenario, the HSSCC mixture S20F10M10 offers the advantage of being used as an improved mechanically sound and environmentally friendly concrete. This study closely aligns with Khodabakhshian et al. (2018), indicating a notable reduction in global warming potential (GWP) indices with escalating incorporation ratios of MWP and SF.

5 Conclusion

High-strength self-compacting concrete (HSSCC) may greatly benefit from the partial substitution of cement with marble powder (MP), silica fume (SF), and fly ash

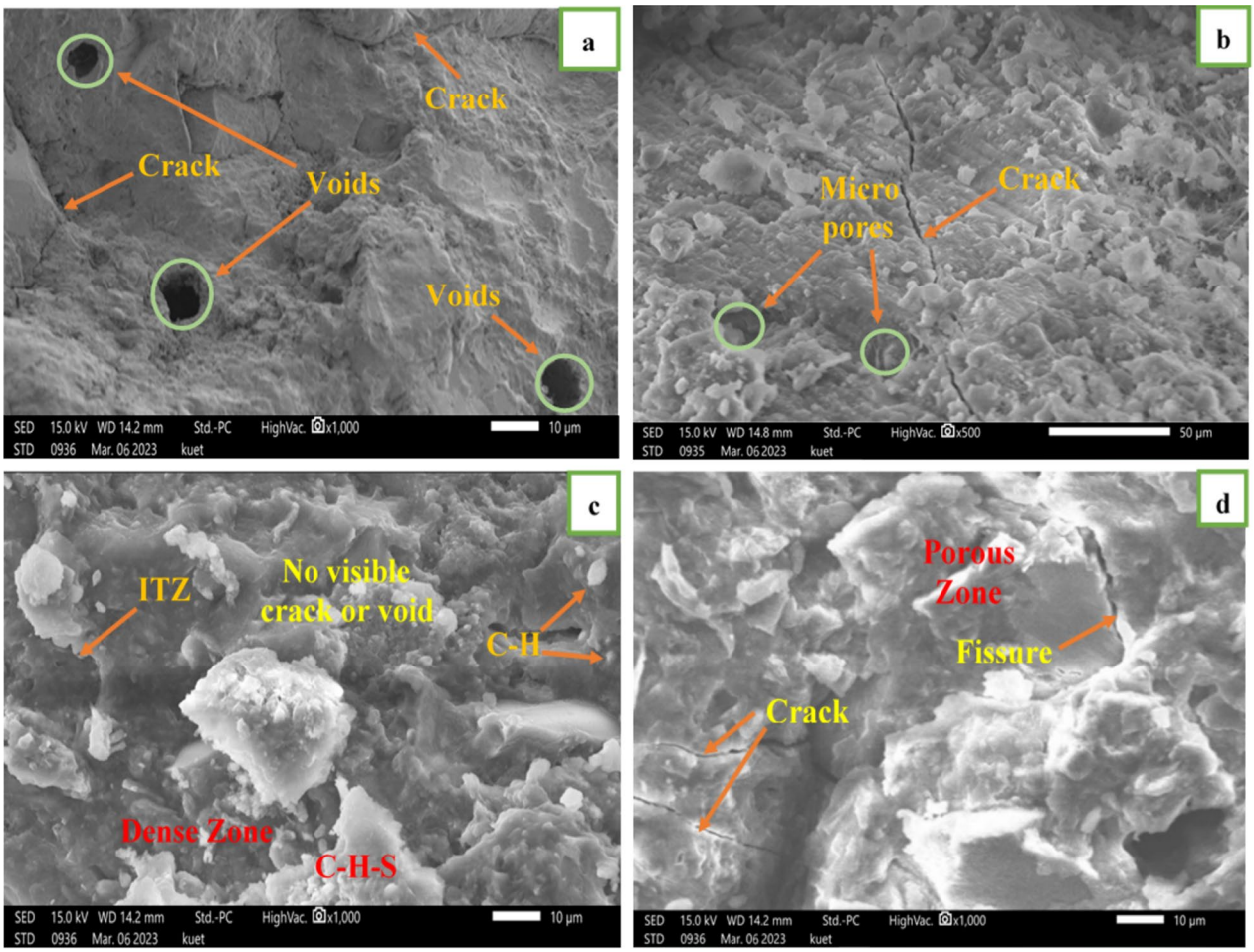

Fig. 19 SEM images of (**a**) S20F0M0 (**b**) S20F10M0 (**c**) S20F10M10 and (**d**) S20F10M20

Table 11 Estimated CO_2 emissions from concrete

Material	CO_2 emission (CO_2-kg/kg)
OPC	0.912 (Yu et al., 2021)
Marble powder	0.082 (Rid et al., 2022)
Silica fume	0.024 (Thilakarathna et al., 2020)
Fly ash	0.027 (Turner & Collins, 2013)
Fine aggregate	0.0139 (Turner & Collins, 2013)
Coarse aggregate	0.0409 (Turner & Collins, 2013)
Water	0.000196 (Yang et al., 2013)
Superplasticizer	0.720 (Long et al., 2015)

(FA). Based on the findings of the experiment, the following inferences may be concluded:

- Combining SF, FA, and MP facilitates the development of HSSCC. The collective use of these SCMs was highlighted to enhance HSSCC's workability, leading to higher flowability and filling ability in the context of fresh characteristics. Evidence also revealed that SCM additions reduced concrete water requirements, resulting in enhanced density.
- Regarding durability characteristics, including MP, SF, and FA significantly reduced the water penetration depth and absorption rate. In the RCPT test, the charge that was transmitted on the concrete was in the low to very low range, which could have further reduced its porosity.
- S20F10M10 demonstrated increases in compressive strength of 10.39, 10.92, and 14.68% on days 7, 28, and 56, respectively, in comparison to the control mix. In terms of splitting tensile strength, it performed 17.32, 15.19, and 15.59% better than the control mix, respectively.
- The ML approach demonstrated the superiority of RF, GB, and their ensemble models in predicting fresh and mechanical characteristics. While GB and ensemble models have shown more reliability than RF algorithms across various statistical evaluations,

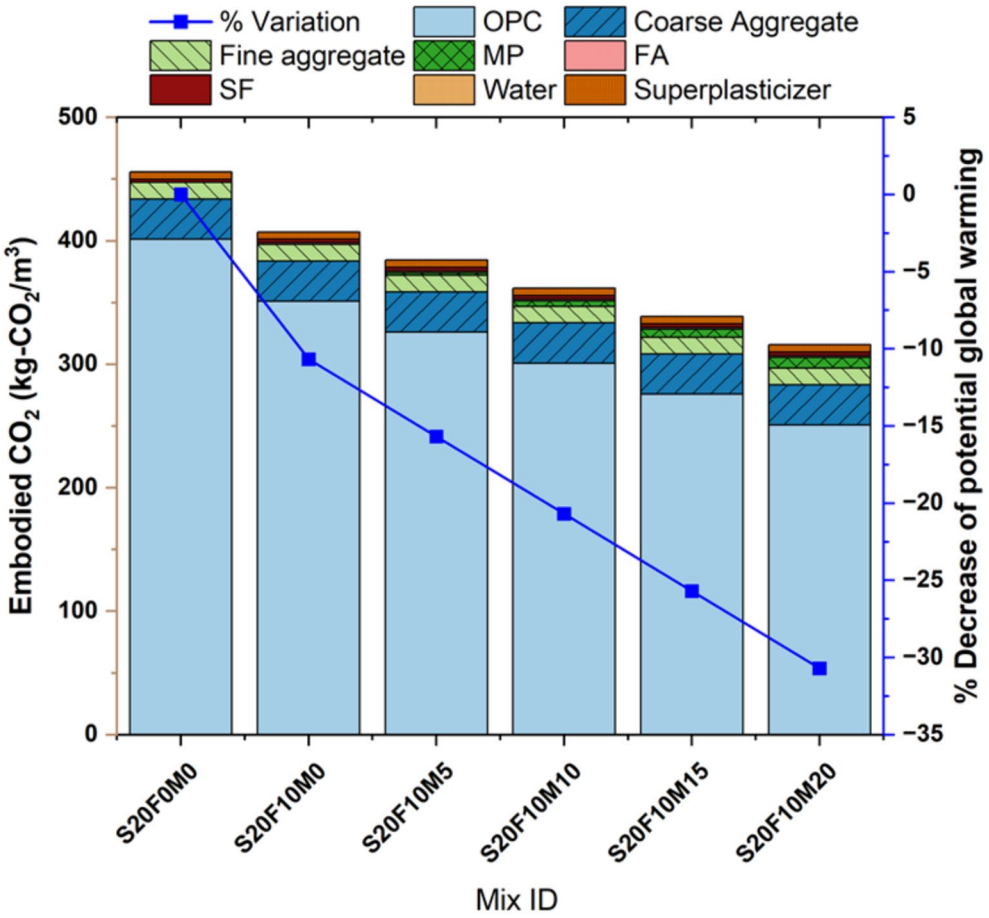

Fig. 20 The entire CO_2 emissions and possible global warming reduction percentage

RF algorithms remain viable for forecasting concrete strength.

- The replacement of 10% MP to a steady 10% FA and 20% SF resulted in UPV values above 4.5 km/s and rebound index values between 30 and 40, which indicates excellent quality and substantial compressive strength.
- The SEM images of HSSCC generated with a combination of 10% MP, 20% SF, and 10% FA revealed negligible voids, superior aggregate packing, more effective cement paste, and a dense concrete matrix.
- The HSSCC mixture S20F10M10 reduced CO_2 emissions without sacrificing mechanical efficiency.

Supplementary Information

The online version contains supplementary material available at https://doi.org/10.1186/s40069-024-00707-7.

Supplementary Material 1.

Supplementary Material 2.

Acknowledgements
The work was carried out at the Structural and Materials Engineering laboratory of the Department of Building Engineering and Construction Management, Khulna University of Engineering and Technology, Khulna—9203, Bangladesh. The authors would also like to thank the lab technicians who contributed invaluable assistance throughout the research process.

Author contributions
Habibur Rahman Sobuz: Conceptualization, Methodology, Validation, Supervision, Writing - review & editing. Fahim Shahriyar Aditto: Conceptualization, Methodology, Formal analysis, Investigation, Software, Writing - original draft, Writing - review & editing. Shuvo Dip Datta: Validation, Supervision, Writing-original draft, Writing - review & editing. Md. Kawsarul Islam Kabbo: Formal analysis, Writing - review & editing. Jannat Ara Jabin: Formal analysis. S. M. Arifur Rahman: Writing - review & editing. Ahmad Akib Uz Zaman: Data curation.

Data availability
Data will be made available on request.

Author details
[1]Department of Building Engineering and Construction Management, Khulna University of Engineering & Technology, Khulna 9203, Bangladesh. [2]Faculty of Engineering & Quantity Surveying, INTI International University (INTI-IU), Persiaran Perdana BBN, Putra Nilai, Nilai 71800, Negeri Sembilan, Malaysia. [3]Department of Building Engineering and Construction Management, Khulna University of Engineering & Technology, Khulna 9203, Bangladesh. [4]Civil Engineering Discipline, School of Civil and Mechanical Engineering, Curtin University, Perth, WA 6102, Australia. [5]Department of Civil and Architectural

Engineering and Construction Management, University of Wyoming, Laramie, WY 82071, USA.

Received: 27 November 2023 Accepted: 26 June 2024
Published online: 01 October 2024

References

Acikgenc Ulas, M. (2023). Development of an artificial neural network model to predict waste marble powder demand in eco-efficient self-compacting concrete. *Structural Concrete, 24*(2), 2009–2022.

Aditto, F. S., Sobuz, M. H. R., Saha, A., Jabin, J. A., Kabbo, M. K. I., Hasan, N. M. S., & Islam, S. (2023). Fresh, mechanical and microstructural behaviour of high-strength self-compacting concrete using supplementary cementitious materials. *Case Studies in Construction Materials, 19*, e02395. https://doi.org/10.1016/j.cscm.2023.e02395

Ahmad, J., Zhou, Z., & Deifalla, A. F. (2023). Self-compacting concrete with partially substitution of waste marble: A review. *International Journal of Concrete Structures and Materials, 17*(1), 25.

Ahmad, W., Ahmad, A., Ostrowski, K. A., Aslam, F., Joyklad, P., & Zajdel, P. (2021). Application of advanced machine learning approaches to predict the compressive strength of concrete containing supplementary cementitious materials. *Materials, 14*(19), 5762.

Al Daoud, E. (2019). Comparison between XGBoost, LightGBM and CatBoost using a home credit dataset. *International Journal of Computer and Information Engineering, 13*(1), 6–10.

Ali, A., Hussain, Z., Akbar, M., Elahi, A., Bhatti, S., Imran, M., Zhang, P., & Leslie Ndam, N. (2022). Influence of marble powder and polypropylene fibers on the strength and durability properties of self-compacting concrete (SCC). *Advances in Materials Science and Engineering, 2022*, 9553382. https://doi.org/10.1155/2022/9553382

Aliabdo, A. A., Abd Elmoaty, A. E. M., & Auda, E. M. (2014). Re-use of waste marble dust in the production of cement and concrete. *Construction and Building Materials, 50*, 28–41. https://doi.org/10.1016/j.conbuildmat.2013.09.005

Aruntaş, H. Y., Gürü, M., Dayı, M., & Tekin, İ. (2010). Utilization of waste marble dust as an additive in cement production. *Materials & Design, 31*(8), 4039–4042. https://doi.org/10.1016/j.matdes.2010.03.036

Asadi Shamsabadi, E., Roshan, N., Hadigheh, S. A., Nehdi, M. L., Khodabakhshian, A., & Ghalehnovi, M. (2022). Machine learning-based compressive strength modelling of concrete incorporating waste marble powder. *Construction and Building Materials, 324*, 126592. https://doi.org/10.1016/j.conbuildmat.2022.126592

Astm, A. C. (2016). Standard Test Method for Pulse Velocity Through Concrete.

Astm, A. (2018). *C33/C33M-18 standard specification for concrete aggregates*. ASTM International.

ASTM-C1585. (2013). 1585–13 "Standard test method for measurement of rate of absorption of water by hydraulic cement concrete". *West Conshohocken*

ASTM-C1202. (2019). *Standard test method for electrical indication of concrete's ability to resist chloride ion penetration*. ASTM International.

ASTM-C1723. (2016). *Standard guide for examination of hardened concrete using scanning electron microscopy*. ASTM International.

ASTM-C192, 192M. C192, C192M-18,". (2018). *Standard practice for making and curing concrete test specimens in the laboratory*. ASTM International.

ASTM-C33. (2003). ASTM C33 standard specifications for concrete aggregates. *ASTM Standard Book*.

ASTM-C39. (2010). Standard test method for compressive strength of cylindrical concrete specimens. *ASTM C39*.

ASTM-C496. (2011). *Standard test method for splitting tensile strength of cylindrical concrete specimens*. American Society for Testing and Materials.

ASTM-C597. (2009). *597, Standard test method for pulse velocity through concrete*. ASTM International.

ASTM-C805. (2018). *ASTM C805–18 standard test method for rebound number of hardened concrete*. ASTM International.

Azimi-Pour, M., Eskandari-Naddaf, H., & Pakzad, A. (2020). Linear and non-linear SVM prediction for fresh properties and compressive strength of high volume fly ash self-compacting concrete. *Construction and Building Materials, 230*, 117021. https://doi.org/10.1016/j.conbuildmat.2019.117021

BDS.EN:197–1. 197–1: 2003. *Bangladesh Standard, Cement-Part*, *1*.

Belagraa, L., Abdelaziz, M., & Miloud, B. (2015). Study of the physico-mechanical properties of a recycled concrete incorporating admixtures by the means of NDT methods. *Procedia Engineering, 108*, 80–92. https://doi.org/10.1016/j.proeng.2015.06.122

Belaidi, A. S. E., Kenai, S., Kadri, E.-H., Soualhi, H., & Benchaâ, B. (2016). Effects of experimental ternary cements on fresh and hardened properties of self-compacting concretes. *Journal of Adhesion Science and Technology, 30*(3), 247–261. https://doi.org/10.1080/01694243.2015.1099864

Belouadah, M., Rahmouni, Z. E., Tebbal, N., & Hicham, M. E. H. (2021). Evaluation of concretes made with marble waste using destructive and non-destructive testing. *Annales De Chimie Science Des Materiaux*. https://doi.org/10.1828/acsm.450501

Breiman, L. (2001). Random forests. *Machine Learning, 45*, 5–32.

Breysse, D. (2012). Nondestructive evaluation of concrete strength: an historical review and a new perspective by combining NDT methods. *Construction and Building Materials, 33*, 139–163. https://doi.org/10.1016/j.conbuildmat.2011.12.103

BS.EN:12350–8. (2010). *BS EN 12350–8: 2010 testing fresh concrete part 8: self-compacting concrete—slump-flow test*. British Standards Institution.

Choudhary, R., Jain, A., & Gupta, R. (2019). Utilization of waste marble powder and silica fume in self-compacting concrete. *UKIERI*, 184–194.

Chung, L., Han, S. H., Choi, J. J., Oh, S. K., Hong, S. G., Lee, J. H., Oh, B., Lee, H.-K., Kwak, H.-G., & Kang, T. (2013). International Journal of Concrete Structures and Materials. *International Journal of Concrete Structures and Materials*, *7*(1).

Datta, S. D., Sarkar, M. M., Rakhe, A. S., Aditto, F. S., Sobuz, M. H. R., Shaurdho, N. M. N., Nijum, N. J., & Das, S. (2024). Analysis of the characteristics and environmental benefits of rice husk ash as a supplementary cementitious material through experimental and machine learning approaches. *Innovative Infrastructure Solutions, 9*(4), 121. https://doi.org/10.1007/s41062-024-01423-7

Datta, S. D., Sobuz, M. H. R., Akid, A. S. M., & Islam, S. (2022). Influence of coarse aggregate size and content on the properties of recycled aggregate concrete using non-destructive testing methods. *Journal of Building Engineering, 61*, 105249. https://doi.org/10.1016/j.jobe.2022.105249

De Almeida, I. R. (1991, 1991). Non-destructive testing of high strength concretes: rebound (Schmidt hammer) and ultra-sonic pulse velocity. Proceedings of 2nd International RILEM/CEB Symposium on Quality control of concrete structures, pp. 387–397.,

de Prado-Gil, J., Zaid, O., Palencia, C., & Martínez-García, R. (2022). Prediction of splitting tensile strength of self-compacting recycled aggregate concrete using novel deep learning methods. *Mathematics, 10*(13), 2245.

Dhiyaneshwaran, S., Ramanathan, P., Baskar, I., & Venkatasubramani, R. (2013). Study on durability characteristics of self-compacting concrete with fly ash. *Jordan Journal of Civil Engineering, 7*(3), 342–353.

Domingo, R., & Hirose, S. (2009). Correlation between concrete strength and combined nondestructive tests for concrete using high-early strength cement. The Sixth Regional Symposium on Infrastructure Development (pp. 12–13).

EFNARC, S.-C. (2005). The European guidelines for self-compacting concrete. *BIBM, et al*, *22*, 563.

El-Chabib, H., & Syed, A. (2013). Properties of self-consolidating concrete made with high volumes of supplementary cementitious materials. *Journal of Materials in Civil Engineering, 25*(11), 1579–1586.

Elyamany, H. E., Abd Elmoaty, A. E. M., & Mohamed, B. (2014). Effect of filler types on physical, mechanical and microstructure of self compacting concrete and Flow-able concrete. *Alexandria Engineering Journal, 53*(2), 295–307. https://doi.org/10.1016/j.aej.2014.03.010

EN.BS:12350–12. (2010). 12350–12 (2010). Testing fresh concrete-Part 12: Selfcompacting concrete-J ring test, Technical standard. *British Standards Institution, England*.

EN.BS-12390–8. (2019). *12390–8: 2019; testing hardened concrete-part 8: depth of penetration of water under pressure*. Brussels: CEN.

Friedman, J. H. (2002). Stochastic gradient boosting. *Computational Statistics & Data Analysis, 38*(4), 367–378.

Gesoğlu, M., Güneyisi, E., & Özbay, E. (2009). Properties of self-compacting concretes made with binary, ternary, and quaternary cementitious blends of fly ash, blast furnace slag, and silica fume. *Construction and Building Materials, 23*(5), 1847–1854. https://doi.org/10.1016/j.conbuildmat.2008.09.015

Givi, A. N., Rashid, S. A., Aziz, F. N. A., & Salleh, M. A. M. (2010). Contribution of rice husk ash to the properties of mortar and concrete: A review. *Journal of American Science, 6*(3), 157–165.

Habibur Rahman Sobuz, M., Khan, M. H., Kawsarul Islam Kabbo, M., Alhamami, A. H., Aditto, F. S., Saziduzzaman Sajib, M., Johnson Alengaram, U., Mansour, W., Hasan, N. M. S., Datta, S. D., & Alam, A. (2024). Assessment of mechanical properties with machine learning modeling and durability, and microstructural characteristics of a biochar-cement mortar composite. *Construction and Building Materials, 411*, 134281. https://doi.org/10.1016/j.conbuildmat.2023.134281

Hasan, N.M.S.; Sobuz, M.H.R.; Khan, M.M.H.; Mim, N.J.; Meraz, M.M.; Datta, S.D.; Rana, M.J.; Saha, A.; Akid, A.S.M.; Mehedi, M.T.; et al. (2022). Integration of Rice Husk Ash as Supplementary Cementitious Material in the Production of Sustainable High-Strength Concrete. *Materials*. https://doi.org/10.3390/ma15228171

Jain, A., Kathuria, A., Kumar, A., Verma, Y., & Murari, K. (2013). Combined use of non-destructive tests for assessment of strength of concrete in structure. *Procedia Engineering, 54*, 241–251. https://doi.org/10.1016/j.proeng.2013.03.022

Jalal, M., Pouladkhan, A., Harandi, O. F., & Jafari, D. (2015). RETRACTED: comparative study on effects of Class F fly ash, nano silica and silica fume on properties of high performance self compacting concrete. *Construction and Building Materials, 94*, 90–104. https://doi.org/10.1016/j.conbuildmat.2015.07.001

Kanellopoulos, A., Petrou, M. F., & Ioannou, I. (2012). Durability performance of self-compacting concrete. *Construction and Building Materials, 37*, 320–325. https://doi.org/10.1016/j.conbuildmat.2012.07.049

Khair, S., Rahman, S. M. A., Shaikh, F. U. A., & Sarker, P. K. (2024). Evaluating lithium slag for geopolymer concrete: a review of its properties and sustainable construction applications. *Case Studies in Construction Materials, 20*, e02822. https://doi.org/10.1016/j.cscm.2023.e02822

Khan, M. M. H., Sobuz, M. H. R., Meraz, M. M., Tam, V. W., Hasan, N. M. S., & Shaurdho, N. M. N. (2023). Effect of various powder content on the properties of sustainable self-compacting concrete. Case Studies in Construction Materials, 19, e02274. https://doi.org/10.1016/j.cscm.2023.e02274

Khodabakhshian, A., de Brito, J., Ghalehnovi, M., & Asadi Shamsabadi, E. (2018). Mechanical, environmental and economic performance of structural concrete containing silica fume and marble industry waste powder. *Construction and Building Materials, 169*, 237–251. https://doi.org/10.1016/j.conbuildmat.2018.02.192

Leung, H. Y., Kim, J., Nadeem, A., Jaganathan, J., & Anwar, M. P. (2016). Sorptivity of self-compacting concrete containing fly ash and silica fume. *Construction and Building Materials, 113*, 369–375. https://doi.org/10.1016/j.conbuildmat.2016.03.071

Lija, R., & Minu, S. (2016). Workability and strength behaviour of self-compacting concrete with silica fume and marble sawing waste. *International Journal of Civil Engineering and Technology, 7*, 474–482.

Long, G., Gao, Y., & Xie, Y. (2015). Designing more sustainable and greener self-compacting concrete. *Construction and Building Materials, 84*, 301–306. https://doi.org/10.1016/j.conbuildmat.2015.02.072

Madandoust, R., Ghavidel, R., & Nariman-zadeh, N. (2010). Evolutionary design of generalized GMDH-type neural network for prediction of concrete compressive strength using UPV. *Computational Materials Science, 49*(3), 556–567. https://doi.org/10.1016/j.commatsci.2010.05.050

Mahmood, M. S., Elahi, A., Zaid, O., Alashker, Y., Şerbănoiu, A. A., Grădinaru, C. M., Ullah, K., & Ali, T. (2023). Enhancing compressive strength prediction in self-compacting concrete using machine learning and deep learning techniques with incorporation of rice husk ash and marble powder. *Case Studies in Construction Materials, 19*, e02557. https://doi.org/10.1016/j.cscm.2023.e02557

Md, P. J. (2019). Strength and durability studies on steel fibre reinforced self compacting concrete. *CVR Journal of Science and Technology, 17*(1), 1–7.

Meera, M., Dash, A. K., & Gupta, S. (2020). Rheological and strength properties of self-compacting concrete incorporating marble and granite powders. *Materials Today: Proceedings, 32*, 1005–1013. https://doi.org/10.1016/j.matpr.2020.08.531

Raghunath, P. N., Suguna, K., Karthick, J., & Sarathkumar, B. (2019). Mechanical and durability characteristics of marble-powder-based high-strength concrete. *Scientia Iranica, 26*(6), 3159–3164. https://doi.org/10.2420/sci.2018.4953.1005

Rahman, S. A., Dodd, A., Khair, S., Shaikh, F. U. A., Sarker, P. K., & Hosan, A. (2023b). Assessment of lithium slag as a supplementary cementitious material: pozzolanic activity and microstructure development. *Cement and Concrete Composites*. https://doi.org/10.1016/j.cemconcomp.2023.105262

Rahman, S., Mahmood, A. H., Shaikh, F. U. A., & Sarker, P. K. (2023a). Fresh state and hydration properties of high-volume lithium slag cement composites. *Materials and Structures, 56*(4), 1–19.

Rahman, S. A., Shaikh, F. U. A., & Sarker, P. K. (2022). A comprehensive review of properties of concrete containing lithium refinery residue as partial replacement of cement. *Construction and Building Materials, 328*, 127053.

Rahman, S. A., Shaikh, F. U. A., & Sarker, P. K. (2024). Fresh, mechanical, and microstructural properties of lithium slag concretes. *Cement and Concrete Composites*. https://doi.org/10.1016/j.cemconcomp.2024.105469

Rahman Sobuz, M. H., Meraz, M. M., Safayet, M. A., Mim, N. J., Mehedi, M. T., Noroozinejad Farsangi, E., Shrestha, R. K., Kader Arafin, S. A., Bibi, T., Hussain, M. S., Bhattacharya, B., Aftab, M. R., Paul, S. K., Paul, P., & Meraz, M. M. (2023). Performance evaluation of high-performance self-compacting concrete with waste glass aggregate and metakaolin. *Journal of Building Engineering, 67*, 105976. https://doi.org/10.1016/j.jobe.2023.105976

Rid, Z. A., Shah, S. N. R., Memon, M. J., Jhatial, A. A., Keerio, M. A., & Goh, W. I. (2022). Evaluation of combined utilization of marble dust powder and fly ash on the properties and sustainability of high-strength concrete. *Environmental Science and Pollution Research, 29*(19), 28005–28019. https://doi.org/10.1007/s11356-021-18379-1

Sadek, D. M., El-Attar, M. M., & Ali, H. A. (2016). Reusing of marble and granite powders in self-compacting concrete for sustainable development. *Journal of Cleaner Production, 121*, 19–32.

Sardinha, M., de Brito, J., & Rodrigues, R. (2016). Durability properties of structural concrete containing very fine aggregates of marble sludge. *Construction and Building Materials, 119*, 45–52. https://doi.org/10.1016/j.conbuildmat.2016.05.071

Sharma, R., & Khan, R. A. (2017a). Durability assessment of self compacting concrete incorporating copper slag as fine aggregates. *Construction and Building Materials, 155*, 617–629. https://doi.org/10.1016/j.conbuildmat.2017.08.074

Sharma, R., & Khan, R. A. (2017b). Sustainable use of copper slag in self compacting concrete containing supplementary cementitious materials. *Journal of Cleaner Production, 151*, 179–192. https://doi.org/10.1016/j.jclepro.2017.03.031

Sideris, K. K., & Anagnostopoulos, N. S. (2013). Durability of normal strength self-compacting concretes and their impact on service life of reinforced concrete structures. *Construction and Building Materials, 41*, 491–497. https://doi.org/10.1016/j.conbuildmat.2012.12.042

Silva, P. F. S., Moita, G. F., & Arruda, V. F. (2020). Machine learning techniques to predict the compressive strength of concrete. *Revista Internacional De Métodos Numéricos Para Cálculo y Diseño En Ingeniería*. https://doi.org/10.2396/j.rimni.2020.09.008

Singh, M., Srivastava, A., & Bhunia, D. (2017). An investigation on effect of partial replacement of cement by waste marble slurry. *Construction and Building Materials, 134*, 471–488.

Sunayana, S., & Barai, S. V. (2017). Recycled aggregate concrete incorporating fly ash: comparative study on particle packing and conventional method. *Construction and Building Materials, 156*, 376–386. https://doi.org/10.1016/j.conbuildmat.2017.08.132

Tennich, M., Kallel, A., & Ben Ouezdou, M. (2015). Incorporation of fillers from marble and tile wastes in the composition of self-compacting concretes. *Construction and Building Materials, 91*, 65–70. https://doi.org/10.1016/j.conbuildmat.2015.04.052

Tennich, M., Ouezdou, M. B., & Kallel, A. (2017). Behavior of self-compacting concrete made with marble and tile wastes exposed to external sulfate attack. *Construction and Building Materials, 135*, 335–342.

Thilakarathna, P. S. M., Seo, S., Baduge, K. S. K., Lee, H., Mendis, P., & Foliente, G. (2020). Embodied carbon analysis and benchmarking emissions of high and ultra-high strength concrete using machine learning algorithms. *Journal of Cleaner Production, 262*, 121281. https://doi.org/10.1016/j.jclepro.2020.121281

Turner, L. K., & Collins, F. G. (2013). Carbon dioxide equivalent (CO2-e) emissions: a comparison between geopolymer and OPC cement concrete. *Construction and Building Materials, 43*, 125–130. https://doi.org/10.1016/j.conbuildmat.2013.01.023

Uysal, M., & Sumer, M. (2011). Performance of self-compacting concrete containing different mineral admixtures. *Construction and Building Materials, 25*(11), 4112–4120. https://doi.org/10.1016/j.conbuildmat.2011.04.032
Uysal, M., & Tanyildizi, H. (2012). Estimation of compressive strength of self compacting concrete containing polypropylene fiber and mineral additives exposed to high temperature using artificial neural network. *Construction and Building Materials, 27*(1), 404–414. https://doi.org/10.1016/j.conbuildmat.2011.07.028
Uysal, M., & Yilmaz, K. (2011). Effect of mineral admixtures on properties of self-compacting concrete. *Cement and Concrete Composites, 33*(7), 771–776. https://doi.org/10.1016/j.cemconcomp.2011.04.005
Vasusmitha, R., & Rao, P. S. (2013). Strength and durability study of high strength self compacting concrete. *International Journal of Mining, Metallurgy & Mechanical Engineering, 1*(1), 18–26.
Velci Shridevi, P. A., Shahul Hameed, M., Kumar, R., Dhanalakshmi, A., & Mohamed Thameem Ansari, H. (2023). Strength characteristics of fibre reinforced self compacting concrete using marble sludge powder. *Materials Today: Proceedings*. https://doi.org/10.1016/j.matpr.2023.12.004
Vo, D.-H., Yehualaw, M. D., Hwang, C.-L., Liao, M.-C., Tran Thi, K.-D., & Chao, Y.-F. (2021). Mechanical and durability properties of recycled aggregate concrete produced from recycled and natural aggregate blended based on the densified mixture design algorithm method. *Journal of Building Engineering, 35*, 102067. https://doi.org/10.1016/j.jobe.2020.102067
Wongkeo, W., Thongsanitgarn, P., Ngamjarurojana, A., & Chaipanich, A. (2014). Compressive strength and chloride resistance of self-compacting concrete containing high level fly ash and silica fume. *Materials & Design, 64*, 261–269. https://doi.org/10.1016/j.matdes.2014.07.042
Xie, T., Yang, G., Zhao, X., Xu, J., & Fang, C. (2020). A unified model for predicting the compressive strength of recycled aggregate concrete containing supplementary cementitious materials. *Journal of Cleaner Production, 251*, 119752. https://doi.org/10.1016/j.jclepro.2019.119752
Xu, J., Chen, Y., Xie, T., Zhao, X., Xiong, B., & Chen, Z. (2019). Prediction of triaxial behavior of recycled aggregate concrete using multivariable regression and artificial neural network techniques. *Construction and Building Materials, 226*, 534–554. https://doi.org/10.1016/j.conbuildmat.2019.07.155
Yang, K.-H., Song, J.-K., & Song, K.-I. (2013). Assessment of CO2 reduction of alkali-activated concrete. *Journal of Cleaner Production, 39*, 265–272. https://doi.org/10.1016/j.jclepro.2012.08.001
Yong, Y. K., & Lee, H. P. (2022). Palm Oil Fly Ash (POFA) as a Cementitious Material in Biomass Concrete: A Feasibility Review. Inti Journal, 2022(08), 1–12.
Yu, J., Wu, H.-L., Mishra, D. K., Li, G., & Leung, C. K. Y. (2021). Compressive strength and environmental impact of sustainable blended cement with high-dosage limestone and calcined clay (LC2). *Journal of Cleaner Production, 278*, 123616. https://doi.org/10.1016/j.jclepro.2020.123616

Publisher's Note

Md. Habibur Rahman Sobuz Associate Professor at Department of Building Engineering and Construction Management, Khulna University of Engineering & Technology, Khulna - 9203, Bangladesh.

Fahim Shahriyar Aditto Graduate Student at Department of Building Engineering and Construction Management, Khulna University of Engineering & Technology, Khulna - 9203, Bangladesh.

Shuvo Dip Datta Lecturer at Department of Building Engineering and Construction Management, Khulna University of Engineering & Technology, Khulna - 9203, Bangladesh.

Md. Kawsarul Islam Kabbo Lecturer at Department of Building Engineering and Construction Management, Khulna University of Engineering & Technology, Khulna - 9203, Bangladesh.

Jannat Ara Jabin Graduate Student at Department of Building Engineering and Construction Management, Khulna University of Engineering & Technology, Khulna - 9203, Bangladesh.

Md. Munir Hayet Khan Associate Professor at Faculty of Engineering & Quantity Surveying INTI International University (INTI-IU), Persiaran Perdana BBN, Putra Nilai, Nilai 71800, Negeri Sembilan, Malaysia.

S.M. Arifur Rahman PhD Scholar at Civil Engineering Discipline, School of Civil and Mechanical Engineering, Curtin University, Perth, WA 6102, Australia

Mehernaz Raazi Graduate Student at Department of Building Engineering and Construction Management, Khulna University of Engineering & Technology, Khulna - 9203, Bangladesh.

Ahmad Akib Uz Zaman Post-graduate Student, Department of Civil and Architectural Engineering and Construction Management, University of Wyoming, Laramie, WY 82071, United States.